

# Influence of permafrost type and site history on losses of permafrost carbon after thaw

Kristen Manies<sup>1</sup>, Miriam C Jones<sup>1</sup>, Mark P Waldrop<sup>1</sup>, Mary-Cathrine Leewis<sup>2</sup>, Christopher Fuller<sup>3</sup>, Robert Cornman<sup>4</sup>, and Kristen Hoefke<sup>4</sup>

<sup>1</sup>United States Geological Survey

<sup>2</sup>USGS

<sup>3</sup>US Geological Survey

<sup>4</sup>U.S. Geological Survey

November 23, 2022

## Abstract

We quantified permafrost plateau and post-thaw carbon (C) stocks across a peatland permafrost thaw chronosequence in Interior Alaska to evaluate the amount of C loss with thaw. Peat core macrofossil reconstructions revealed three stratigraphic layers of peat: (1) a base layer of fen/marsh peat, (2) forested permafrost plateau peat and, (3) collapse-scar bog peat (at sites where permafrost thaw has occurred). Radiocarbon dating revealed that peat initiated at all sites within the last 2,500 years and that permafrost aggraded during the Little Ice Age (ca. 250 – 575 years ago) and degraded within the last several decades. We found the timing of permafrost thaw within each feature was not related to thaw bog size, as hypothesized. Their rate of expansion may be more influenced by local factors, such as ground ice content and subsurface water inputs. We found C losses due to thaw for the century of approximately 34% of the C available, but the absolute amount of C lost ( $\text{kg m}^{-2}$ ) was over 50% lower than losses previously described in other Alaskan peatland chronosequences. We hypothesize that the difference stems from the process by which permafrost aggraded, with sites that formed permafrost epigenetically (significantly later than the majority of peat accumulation) experiencing less C loss with thaw than sites that formed syngenetically (simultaneously with peat accumulation). We suggest that C:N ratios can provide a first order estimate of how much peat has been processed prior to permafrost aggradation, helping to predict the magnitude of C loss with thaw.

1 **Influence of permafrost type and site history on losses of permafrost carbon after thaw**

2

3 Kristen L. Manies<sup>1\*</sup>, Miriam C. Jones<sup>2</sup>, Mark P. Waldrop<sup>1</sup>, Mary-Cathrine Leewis<sup>1</sup>,

4 Christopher Fuller<sup>1</sup>, R. Scott Cornman<sup>3</sup>, and Kristen Hoefke<sup>2</sup>

5 \*Corresponding author

6 <sup>1</sup>U.S. Geological Survey; Geology, Minerals, Energy, and Geophysics Science Center; Menlo Park, CA

7 <sup>2</sup>U.S. Geological Survey; Florence Bascom Geoscience Center; Reston, VA

8 <sup>3</sup>U.S. Geological Survey; Fort Collins Science Center; Fort Collins, CO

9

10 **Key points**

- 11 • Collapse-scar bog ages at our sites were not related to feature size and may have been more  
12 influenced by local factors.
- 13 • We found smaller losses of C with permafrost thaw than other studies from Interior Alaska.
- 14 • The timing of permafrost aggradation relative to peat accumulation is an important factor in  
15 determining how much C is lost with thaw.

16 **Abstract**

17 We quantified permafrost plateau and post-thaw carbon (C) stocks across a peatland permafrost  
18 thaw chronosequence in Interior Alaska to evaluate the amount of C loss with thaw. Peat core  
19 macrofossil reconstructions revealed three stratigraphic layers of peat: (1) a base layer of fen/marsh  
20 peat, (2) forested permafrost plateau peat and, (3) collapse-scar bog peat (at sites where permafrost  
21 thaw has occurred). Radiocarbon dating revealed that peat initiated at all sites within the last 2,500  
22 years and that permafrost aggraded during the Little Ice Age (ca. 250 – 575 years ago) and degraded  
23 within the last several decades. We found the timing of permafrost thaw within each feature was not  
24 related to thaw bog size, as hypothesized. Their rate of expansion may be more influenced by local

25 factors, such as ground ice content and subsurface water inputs. We found C losses due to thaw for the  
26 century of approximately 34% of the C available, but the absolute amount of C lost ( $\text{kg m}^{-2}$ ) was over  
27 50% lower than losses previously described in other Alaskan peatland chronosequences. We  
28 hypothesize that the difference stems from the process by which permafrost aggraded, with sites that  
29 formed permafrost epigenetically (significantly later than the majority of peat accumulation)  
30 experiencing less C loss with thaw than sites that formed syngenetically (simultaneously with peat  
31 accumulation). We suggest that C:N ratios can provide a first order estimate of how much peat has been  
32 processed prior to permafrost aggradation, helping to predict the magnitude of C loss with thaw.

### 33 **Plain Language Summary**

34 We quantified peat carbon at a permafrost peatland in Alaska to see how much carbon was lost from  
35 the peat when permafrost, or frozen soil, thawed and that area became a collapse-scar bog. We found  
36 that size of the bog was unrelated to its age. Factors such as the amount of ice in the soil and water  
37 entering the bogs from the surrounding forests may have been more important in determining their  
38 growth. We did not find as large of losses of carbon from as found at other Alaskan sites. We compared  
39 our results to other studies, some which had small losses of carbon due to thaw, others which found  
40 large losses. We found that factors related to time (i.e., age of landform, number of years the site had  
41 permafrost) are important but don't fully explain these different results. However, when we include  
42 how permafrost formed we see a trend: sites where permafrost formed after peat (epigenetic  
43 permafrost) had smaller carbon losses than sites where permafrost and peats formed at the same time  
44 (syngenetic permafrost). Determining permafrost type can be difficult; instead scientists can use C:N  
45 ratios to determine if their samples resemble peat formed by epigenetic versus syngenetic permafrost.

## 46 1.0 Introduction

47 Northern peatlands play an important role in the global carbon (C) budget and are estimated to  
48 store 415 Pg of C (+/- 150 Pg C; Hugelius et al., 2020), which represents approximately 20 % of the global  
49 soil C stock (Jackson et al., 2017). Close to half of this C has been protected from decomposition by  
50 permafrost, substrate that has remained frozen for at least two consecutive years (Rodenhizer et al.,  
51 2020). Permafrost in northern peatlands reached its maximum extent around 1700 Common Era (CE),  
52 with the highest rates of aggradation between 1200 - 1950 CE (Treat & Jones, 2018). Much of this  
53 permafrost is found in the discontinuous zone, where areas of permafrost are found adjacent to areas of  
54 unfrozen soil. In the discontinuous zone, the majority of which resides above 60 °N (Brown et al., 1997),  
55 the presence of permafrost depends on the area's climate (both past and present) as well as local  
56 factors, such as vegetation, aspect, thickness of organic soil horizons, and texture of the mineral soil  
57 (Shur & Jorgenson, 2007). Permafrost can form either after the deposition of peat/sediments  
58 (epigenetic permafrost) or concurrent with peat/sediment deposition (syngenetic permafrost). Between  
59 2.20 – 3.95 10<sup>6</sup> km<sup>2</sup> of the northern hemisphere is estimated to have discontinuous permafrost (Zhang  
60 et al., 2000).

61 Permafrost peatlands within the discontinuous zone are often associated with forested peat  
62 plateaus (Gibson et al., 2019). Typically, these ecosystems are vegetated with black spruce (*Picea*  
63 *mariana*) trees and ericaceous shrubs, such as Labrador Tea (*Rhododendron groenlandicum*), with a  
64 ground cover of feathermosses and *Sphagnum* spp. The underlying organic soil, or peat, can be up to 6  
65 m thick (Gibson et al., 2019). The uppermost peat, known as the active layer, undergoes seasonal  
66 freezing and thawing and is usually 0.3 – 0.7 m thick, with permafrost found below (Shur et al., 2011).  
67 Microbial decomposition of organic matter (OM) in this frozen soil is dramatically reduced compared to  
68 unfrozen soils, thereby stabilizing a large pool of potentially labile C (Harden et al., 2012; Leewis et al.,

69 2020). Once thawed, this reserve of C is available for more rapid decomposition, which results in losses  
70 of C from the soil, much of which is lost to the atmosphere.

71 Over the past few decades, air temperatures within the northern high latitudes have warmed at  
72 a faster rate than other locations around the globe (Oliva & Fritz, 2018). These changes have increased  
73 soil temperatures (Jungqvist et al., 2014), growing-season length (Euskirchen et al., 2009), and both fire  
74 frequency and intensity (Turetsky et al., 2011), all of which impact permafrost stability and C storage  
75 within these landscapes. In well drained sites, post-thaw conditions usually result in water draining from  
76 the soil, resulting in oxic soil conditions (Estop-Aragonés et al., 2018a). However, permafrost thaw in  
77 lowlands often results in subsidence and inundation, changing the ecosystem from a relatively dry  
78 forested permafrost plateau to bogs or fens with a near-surface water table (Schuur et al., 2015),  
79 resulting in a soil profile that is primarily anaerobic or microaerobic.

80 In lowlands, transitioning from a forested peat plateau to an inundated wetland impacts C  
81 cycling in several ways. First, this transition results in wholesale changes in vegetation; trees die as their  
82 roots become inundated with ground subsidence, resulting in a shift in dominance to inundation-  
83 tolerant *Sphagnum* and/or *Carex* spp. (Finger et al., 2016). Increases in the amount of *Sphagnum*  
84 impacts C accumulation rates (Thormann et al., 1999), as *Sphagnum* is known to reduce decomposition  
85 through lowered pH and creation of decay resistant litter (Malmer et al., 2003). In addition, although  
86 thawed OM is more available to microbial decomposition, inundation creates an anaerobic low nutrient  
87 environment, which shifts microbial populations towards less efficient anaerobic metabolism and the  
88 production of CH<sub>4</sub> rather than CO<sub>2</sub> (Treat et al., 2014). When present, *Carex* spp. are known to increase  
89 diffusion of these gases to the atmosphere from deeper in the soil profile through their aerenchymatous  
90 tissues (Waldo et al., 2019).

91 Permafrost thaw and the formation of collapse scar bogs alters net ecosystem exchange (NEE),  
92 as evidence by the amount of C stored within peat. Some studies have found large C losses from thawed

93 permafrost peat (Jones et al., 2017; O'Donnell et al., 2012) and suggest that it may take centuries to  
94 millennia for these C stocks to recover to their pre-thaw stocks. However, other studies have shown  
95 little C loss from previously frozen peat (Estop-Aragonés et al., 2018a; Heffernan et al., 2020), such that  
96 these losses could be relatively quickly offset by post-thaw peat accumulation. To further understand  
97 the factors which might determine the magnitude of C lost upon permafrost thaw, this study examines C  
98 losses for a new thaw chronosequence situation within forested permafrost plateaus at a site located in  
99 Interior Alaska. We calculate the amount of C loss with thaw for this site and examine these results in  
100 context of other similar studies to understand the factors driving C loss rates.

## 101 **2.0 Methods**

### 102 *2.1 Site information*

103 This study took place in the Alaska Peatland Experiment (APEX; Figure 1), located within the  
104 lowlands of the Bonanza Creek Long-term Ecological Research (LTER) site, on the northwest side of the  
105 Tanana River, a glacially fed braided river. The average annual temperature for this part of Interior  
106 Alaska is -2.4 °C (1981 – 2010), with the average January and July temperatures being -22.2 °C and 16.9  
107 °C, respectively (<https://www.ncdc.noaa.gov/cdo-web/datatools/normals>; Fairbanks, AK). This region  
108 receives ~285 mm of precipitation per year, with about one-third occurring during the winter months  
109 (Hinzman et al., 2006). This region is also within the area of discontinuous permafrost; therefore,  
110 permafrost tends to be found on north facing slopes, valley bottoms, and lowlands (Brown & Kreig,  
111 1983).

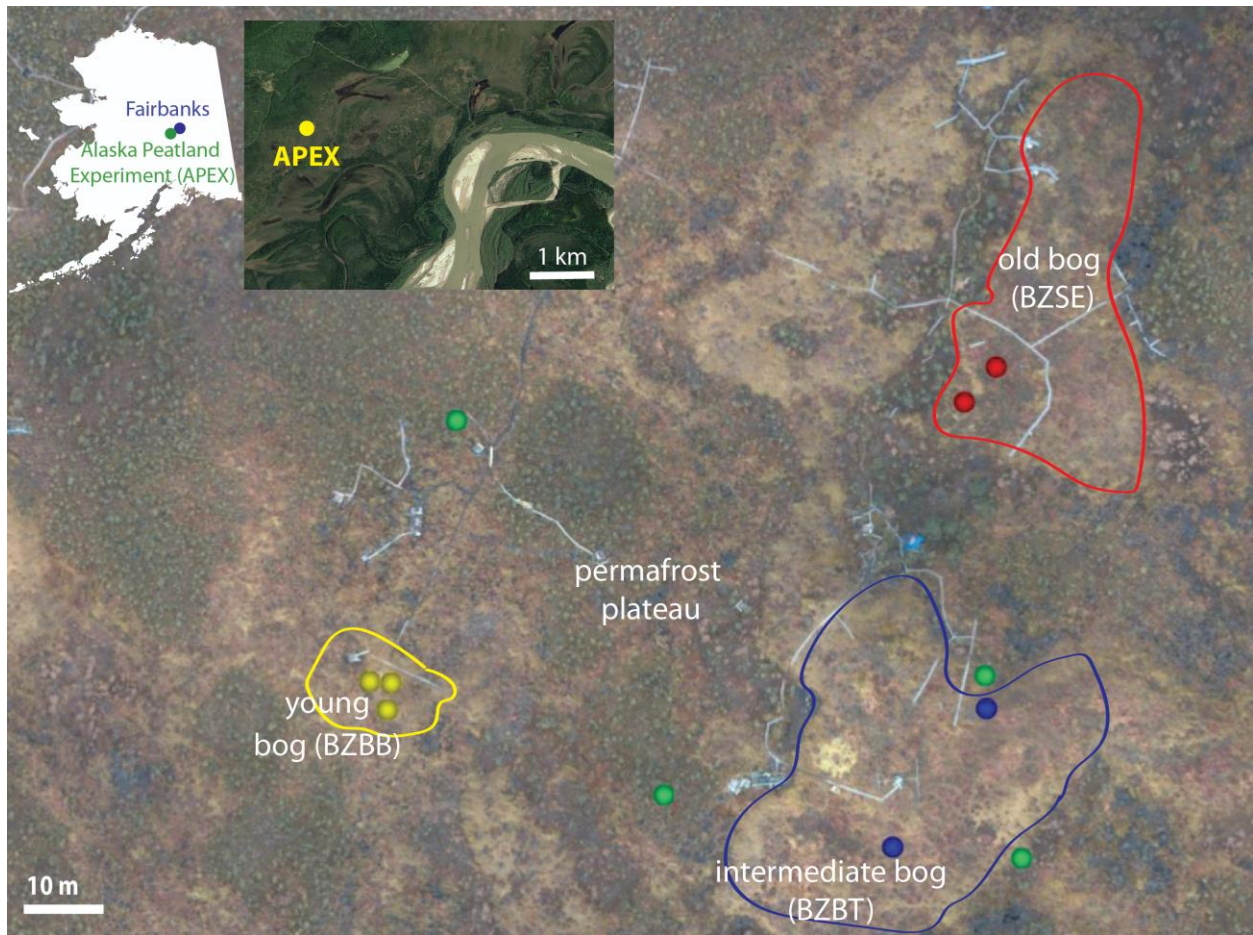
112 The study area is dominated by forested permafrost peat plateaus, covered with *Picea mariana*,  
113 ericaceous shrubs, feather mosses, and occasional *Eriophorum* spp. in the wetter areas. These plateaus  
114 are broken up by collapse-scar bogs of varying sizes (5 – 15,000 m<sup>2</sup>). Collapse-scar bogs form when  
115 localized permafrost thaws; these wetlands remain surrounded by permafrost plateaus, with deeper  
116 permafrost below, isolating the thawed bog from groundwater. Vegetation of these bogs is

117 characterized by diverse *Sphagnum* and *Carex* spp. plants. We examined three thaw features within the  
118 study area, assumed to have thawed at different times in the past based on their size and surface  
119 vegetation. One thaw feature ( $\sim 1,300 \text{ m}^2$ ), with no visible dead trees, was assumed to have thawed  
120 longer ago (Figure 1, red outline, BZSE) than a second feature ( $\sim 2,000 \text{ m}^2$ ) that had drunken or dead  
121 trees on the surface (Figure 1, blue outline, BZBT). A much smaller feature ( $\sim 50 \text{ m}^2$ ) was assumed to  
122 have initiated thaw within the past few decades (Figure 1, yellow outline, BZBB). These sites were  
123 assumed to represent a chronosequence of thaw, ranging from “old” (thaw thought to occur over  
124 centuries), “intermediate” (thaw over decades), and “young” (thaw within the past decade) bogs,  
125 following previous chronosequence studies (Jones et al., 2017; O'Donnell et al., 2012).

## 126 *2.2 Soil core collection and analysis*

127 Two to four cores were collected at each site, with method depending upon ecosystem type and time of  
128 sampling. Frozen soil was cored with a Snow, Ice, and Permafrost Research Establishment (SIPRE) corer  
129 ( $\sim 7.6 \text{ cm}$  diameter; Rand & Mellor, 1985). Unfrozen material was usually collected using a ‘frozen  
130 finger’. Here, a thin-walled, hollow aluminum tube ( $\sim 6.5 \text{ cm}$  diameter), sealed at one end, was inserted  
131 into the peat to the mineral soil. A slurry of dry ice and ethanol was poured into the corer, freezing the  
132 surrounding material to the outside of the corer. After removal the exterior of the core was scraped to  
133 remove large roots and any foreign material that became frozen to the core during removal. Both SIPRE  
134 cores and frozen finger cores were taken to at least the peat-mineral soil boundary. Because the frozen  
135 finger corer did not always recover the surface  $\sim 20 \text{ cm}$  of peat very well, we sometimes sampled surface  
136 material by removing the surface peat in blocks of known dimensions (peat monolith). When more than  
137 one method was used to collect a core, sample data were later combined to represent an entire soil  
138 profile. In all cases, cores were subsampled into 2 to 5 cm depth increments.

139 Processing steps for each subsample depended on the type of sample. Most SIPRE subsamples,  
140 which were a circular disk-shape, were divided into four quadrants used for: 1) chemistry (C, nitrogen



141  
 142 **Figure 1.** The Alaskan Peatland Experiment (APEX) site. This area is a mosaic of collapse-scar bogs within  
 143 forested permafrost plateaus. Colors correspond to the different bogs: the 'old' bog is in red (BZSE), the  
 144 'intermediate' bog is in blue (BZBT), and the 'young' bog is in yellow (BZBB). Circles indicate the locations  
 145 of the soil cores; green circles are cores taken from the permafrost plateau. Core numbers can be found in  
 146 Figure S2. APEX is located near Fairbanks, close to the Tanana River, in the Interior of Alaska. Images: site  
 147 - J. Hollingsworth; satellite – Google Earth.

148 (N), and  $^{210}\text{Pb}$ ) and bulk density, 2) macrofossil and  $^{14}\text{C}$  analysis, 3) DNA-based plant community  
 149 assessment, and 4) an archive. Volume of the bulk density quadrant was determined by first calculating  
 150 the area the quadrant ( $0.25 \times \text{area of a circle}$ ) averaging several measurements of the radius (using  
 151 digital calipers) and multiplying this value by the average of several measurements of the disk  
 152 thickness. Bulk density samples were then weighed, oven dried ( $65\text{ }^\circ\text{C}$  for organic samples, estimated to  
 153 have  $> 20\%$  OM;  $105\text{ }^\circ\text{C}$  for mineral soils), weighed again, and ground to pass through a  $0.25\text{ mm}$  screen  
 154 for further analyses (see following paragraph). For other SIPRE subsamples the disk was trimmed into

155 the shape of a rectangle, the dimensions of which were measured using digital calipers, with the  
156 remainder of the core saved for other analyses and an archive. Frozen finger samples had at least three  
157 small rectangular cubes cut from the larger sample, the dimensions of which were measured using  
158 digital calipers. The remainder of the frozen finger subsample was split between macrofossil analyses  
159 and an archive. The rectangular prisms from both the SIPRE and the frozen finger methods were dried  
160 and ground in the same manner as described above. Regardless of sample collection method, all  
161 samples were described using visual and tactical factors such as level of decomposition, color, and root  
162 abundance. Based on these descriptions they were assigned a horizon designation: live moss (L), dead  
163 moss (D), fibric (mostly undecomposed plant material, F), mesic (more decomposed plant material, M),  
164 humic (very decomposed plant material, H), and mineral soil (Min) based on Manies et al. (2020).

165         The chemistry sample was analyzed for total C and N using a Carlo Erba NA1500 elemental  
166 analyzer (ThermoScientific, Waltham, MA). Samples were combusted in the presence of excess oxygen.  
167 The resulting sample gases were carried by a continuous flow of helium through an oxidation furnace,  
168 followed by a reduction furnace, to yield CO<sub>2</sub>, N<sub>2</sub>, and water vapor. Water was removed by a chemical  
169 trap and CO<sub>2</sub> and N<sub>2</sub> were chromatographically separated before the quantification of C and N (Pella,  
170 1990a, 1990b). Because carbonates are generally absent in this area and pH values were generally less  
171 than 6.0, it was assumed that there was no inorganic carbon present in the mineral soil samples (Soil  
172 Survey Staff, 1951), and, thus, total C represents total organic C. More detailed information regarding  
173 sample processing for samples from the intermediate bog can also be found in Manies et. al (2017). C  
174 storage for each subsample was calculated using C concentration (%), bulk density (g cm<sup>-3</sup>), and  
175 thickness (cm) data. C stocks (kg m<sup>-2</sup>) were calculated as cumulative C storage for all samples between  
176 the moss surface and the organic-mineral soil interface. Examinations of C stocks versus the number of  
177 years for which the core had that stratum (i.e., was a fen, had permafrost) were performed using the *nls*  
178 and *lm* commands in R (R Core Team, 2017).

179 To date surface soil layers, we measured both  $^{14}\text{C}$  in plant macrofossils (see below) and  $^{210}\text{Pb}$  in  
180 bulk soil.  $^{210}\text{Pb}$ , bound to aerosols and dust particles, has been deposited on the land surface from  
181 atmospheric fallout, largely during precipitation events. Age dating using this radionuclide assumes that  
182  $^{210}\text{Pb}$  does not migrate downward within the soil profile over time, so that the activity found at depth  
183 reflects its decay since time of deposition. To examine if  $^{210}\text{Pb}$  was migrating we collected additional  
184 surface soil samples for which we measured both  $^{210}\text{Pb}$  and  $^7\text{Be}$ . Because  $^7\text{Be}$  is also deposited  
185 atmospherically but has a much shorter half-life (53 days versus 22 years), we used  $^7\text{Be}$  as a tracer to  
186 estimate the amount of downward transport, or “downwash”, of  $^{210}\text{Pb}$ . Radionuclides  $^{210}\text{Pb}$ ,  $^{226}\text{Ra}$ ,  $^{137}\text{Cs}$ ,  
187 and  $^7\text{Be}$  were measured on dried, ground samples (2 to 5 cm thick intervals) using gamma spectrometry  
188 following methods described in Van Metre and Fuller (2009). Samples from each soil profile were  
189 measured until unsupported  $^{210}\text{Pb}$ , defined as the activity greater than the activity of its long-lived  
190 parent  $^{226}\text{Ra}$ , was not detected. Unsupported  $^{210}\text{Pb}$  is largely from atmospheric deposition. The Constant  
191 Rate of Supply (CRS) method was used to calculate ages and associated uncertainties from unsupported  
192  $^{210}\text{Pb}$  and were calculated as a function of cumulative dry mass ( $\text{g cm}^{-2}$ ) instead of depth to account for  
193 compaction (Van Metre & Fuller, 2009). Although  $^{137}\text{Cs}$  was measured (data available in Manies et al.,  
194 2021), it was not used to date soil layers due its mobility in acidic peat and potential biological uptake by  
195 vegetation (Turetsky et al., 2004).

### 196 *2.3 Macrofossil analysis*

197 Plant macrofossil assemblages were used as evidence for transitions from one state to another,  
198 such as a forested permafrost plateau to a collapse-scar bog. Approximately 2 cc of sample was washed  
199 through a 250  $\mu\text{m}$  screen using deionized water and examined under a microscope to identify dominant  
200 peat types using semi-quantitative methods (Yu et al., 2010). Relative abundances of herbaceous,  
201 ligneous, and bryophytic peat were estimated and seeds, needles, leaves, and other distinct plant  
202 macrofossils were tallied. Based on characteristics of macrofossil assemblages (Treat et al., 2016), we

203 classified the peat into several categories: 1) 'herbaceous'-dominated peat, containing remains of  
204 Cyperaceae (sedges); 2) 'ligneous' (woody) peat assemblages, which included evidence for taxa such as  
205 black spruce (*Picea mariana*), shrubs, and bryophyte taxa (e.g., feathermosses) associated with  
206 hummocks; and 3) 'bryophytic' peat, which was dominated by *Sphagnum* and other brown mosses.  
207 Where possible, *Sphagnum* mosses were identified to section level and brown mosses were identified to  
208 genus or species level. Brown mosses were further categorized based on their habitat. For example,  
209 mosses in the Amblystegiaceae family are associated with inundated environments, while feather  
210 mosses, *Tomenthypnum nitens*, and *Aulacomnium palustre* were grouped into a 'dry' (hummock or  
211 permafrost plateau) category. Unidentifiable detritus, or plant remains that were too decomposed to  
212 identify their provenance, was also included when present. Zones of permafrost aggradation (a  
213 transition from fen/marsh peat to permafrost plateau peat, see Results) were identified using a  
214 decrease in herbaceous peat with a corresponding increase in ligneous peat. Zones of permafrost thaw  
215 (collapse scar bog peat) were identified using an increase in bryophytic peat with a corresponding  
216 decrease in ligneous peat. Transitions between peat types were identified using visual inspections of the  
217 macrofossil data and confirmed with CONISS based cluster analysis using the Tilia program, which  
218 clusters samples based on presence and abundance of taxa in each sample (v 2.6.1; Grimm, 1987). Core  
219 sections with "dry" mosses, even in small percentages, were assigned to the permafrost plateau strata.  
220 Note that macrofossil horizon designations are not synonymous with field-based horizon designations  
221 (e.g. fibric, mesic, humic).

222           Macrofossil material was used to obtain radiocarbon ( $^{14}\text{C}$ ) ages of initial peat formation  
223 (landform initiation), permafrost aggradation, and permafrost degradation rates in each core. We picked  
224 terrestrial plant macrofossils (seeds, leaves, needles and charcoal) from the sieved macrofossil samples,  
225 targeting the depths of transition in macrofossil assemblage. The  $^{14}\text{C}$  content of each sample was  
226 measured by accelerator mass spectrometry at either the Lawrence Livermore National Laboratory

227 Center for Accelerator Mass Spectrometry (CAMS) or at Beta Analytic (Miami, FL; see Table S2 for  
228 details). Additional information regarding  $^{14}\text{C}$  processing can be found in Manies et. al (2017).  
229 Radiocarbon ages were calibrated to calendar ages in calendar years before present (cal yr BP; present =  
230 1950 CE) and age models were generated using Bacon v 2.3.9.1 (Blaauw & Christen, 2011).

#### 231 *2.4 C loss over time*

232 Cores can have variable amounts of C in their permafrost strata for two reasons: 1) loss due to  
233 thaw, and 2) differing amounts of time for which a core had permafrost, which affects the total amount  
234 of forest permafrost plateau C that a core was able to accumulate. We accounted for the variable times  
235 for which cores had permafrost in two ways. The first method normalizes the C stocks of thawed cores  
236 based on the amount of time each core was accumulating both fen/marsh and forested permafrost  
237 plateau peat to the longest amount of time a core was recorded as accumulating these peats (2725 yrs).  
238 For example, the time for which the Young-bog 2 core (BB2) was accumulating both fen/marsh and  
239 forested permafrost plateau peat was 2040 yrs, or 75 % of 2725 yrs. Therefore, we increased the C  
240 stocks of the BB2 core by 25%, thus accounting for any differences in stocks that may have occurred due  
241 to differences in time with permafrost, with the assumption that any remaining differences in C stocks  
242 are due to thaw-based C losses. We are calling this process the “Normalized C” method. Confidence  
243 intervals were determined using the R package *plotFit* (Greenwell & Schubert Kabban, 2014).

244 The second method we used to account for C stock differences was also used by Jones et al.  
245 (2017). In this method two linear relationships between C stocks versus time (years with fen and  
246 permafrost peat) are calculated for 1) for the cores for which permafrost is still present, and 2) for the  
247 cores for which permafrost has thawed. The difference between these two slopes indicates the degree  
248 to which C has been lost with thaw. We are calling this process the “slope comparison” method.

249

## 250 2.5 Plant DNA Extraction, Amplification, and Analyses

251 We used DNA based techniques to assess the relative abundance of plant DNA (Alsos et al.,  
252 2016; Taberlet et al., 2006), and compared it to morphologically-based macrofossil count data for four  
253 cores. We tested the usefulness of the DNA based technique as a high throughput option of determining  
254 vegetation transitions from these peat cores, which occurred relatively recently. For each of the four  
255 cores for which both macrofossils and DNA analysis was performed, we extracted total genomic  
256 environmental DNA (eDNA) from 44 samples, between 7-10 subsamples for each core from both above  
257 and below the macrofossil-identified transition from forested peat plateau to bog, along with eight  
258 negative controls (one negative control for each 5 core samples processed). To mitigate the potential for  
259 sample contamination by modern plant DNA, the outer 0.5 cm of each core was scraped off using sterile  
260 tools prior to DNA extraction (sensu Leewis et al., 2020). Prior to core cleaning, all nearby surfaces were  
261 sterilized using 10% bleach followed by 70% ethanol spray. Cores and subsets for DNA extraction were  
262 handled only on sterile aluminum foil and all tools (i.e. scalpels, tweezers, foil) were sterilized prior to  
263 use and between each core; additionally, updraft created by an open Bunsen flame was used to limit  
264 infall of potentially contaminating DNA. Negative controls consisted of sterile molecular grade water in  
265 an open tube near the DNA extraction station and were carried throughout the entire analysis including  
266 DNA extraction, PCR, and sequencing. Whole genome eDNA was extracted from ~0.5 g of permafrost  
267 using the DNeasy PowerSoil Kit (Qiagen, Redwood City, CA) according to the manufacturer's  
268 instructions. All samples were eluted into 30  $\mu$ L of molecular grade water. DNA quantity was assessed  
269 using a PicoGreen dsDNA Assay Kit (Thermo Fisher Scientific Technologies, Wilmington, DE) and  
270 concentrations ranged from 9 to 25 ng  $\mu$ L<sup>-1</sup>. All PCR amplifications were performed with the *g* (5'-  
271 GGGCAATCCTGAGCCAA-3') and *h* (5'-CCATTGAGTCTCTGCACCTATC-3') universal plant primers for the  
272 short and variable P6 loop region of the chloroplast *trnL* intron (Taberlet et al., 2006), with addition of  
273 index adapters as required by the RTSF Genomics Core (

274 notes/amplicon-metagenomic-guide/). The amplification was conducted using the following conditions:  
275 97 °C for 4 min, followed by 35 cycles of 94 °C (45 s), 56.7 °C (45 s), and 72°C (45 s), with a final  
276 extension at 72°C (10 min). The amplification was performed in a 25 µL mixture containing 0.25 µL Taq  
277 (5U, AmpliTaq Gold, Thermo Fisher Scientific), 5 µL 5X buffer, 1.5 µL MgCl<sub>2</sub> (25 mM), 0.5 µL dNTPs (10  
278 mM), 0.25 µL BSA (10 mg mL<sup>-1</sup>), 0.25 µL of each primer (50 µM), 5 µL of DNA template (ca. 5 ng µL<sup>-1</sup>), and  
279 12 µL of nuclease-free water. Amplicons were visualized in a 2 % agarose gel. Amplicons were then  
280 purified using the DNA Clean and Concentrator-5 kit (Zymo Research, Irvine, CA, USA), diluted to a  
281 concentration of 10 to 20 nanogram per µL, and sequenced using Illumina MiSeq platform at the  
282 Research Technology Support Facility (RTSF) Genomics Core, Michigan State University sequencing  
283 facility.

284           Sequence reads were processed using the OBITools software package (Boyer et al., 2016b;  
285 <http://metabarcoding.org/obitools>) with a few modifications. First, forward and reverse reads were  
286 aligned and assembled using *illumina-paired-end* and sequences with alignment quality scores < 40 were  
287 filtered out. Retained reads were then assigned to relevant samples using the *ngsfilter* tool with allowed  
288 primer mismatches of 3 bp and no mismatches allowed in the barcodes. Identical sequences were  
289 merged using *obiuniq*. Using *obigrep*, all sequences with only a single copy or shorter than 10 bp were  
290 filtered from the data. *Obiclean* was used to identify amplification and sequencing errors. The read  
291 trimming was further confirmed by trimming any bases that did not align to NCBI's nucleotide database  
292 with BLASTN (task set to "blastn-short" and low-complexity filtering turned off).

293           Taxonomic assignment of sequences was performed with a local taxonomic reference library  
294 containing arctic and boreal vascular and bryophyte taxa (Alsos et al., 2016), after checking that  
295 reference taxa were consistent with the NCBI taxonomy scheme (accessed February 2019). Reads were  
296 aligned with blastn to the reference database (parameters as described above) and the lowest common  
297 ancestor of all matches with an edit distance of two or less was assigned as the read taxonomy. Edit

298 distance was calculated as the sum of alignment gaps, alignment mismatches, and unaligned bases of  
299 the read, and was used instead of a relative measure (such as percent identity) because *trnL* intron  
300 sequences vary greatly in length (Boyer et al., 2016a).

301 Because of the large variation of values found for individual taxa we combined these data into  
302 families for a CONISS-based cluster analysis using Tilia in the same manner as with the morphological  
303 macrofossil analysis (v 2.6.1; Grimm, 1987). We defined the transition between bog and permafrost  
304 plateau vegetation using this sequence data as the depth at which the CONISS analysis first divided the  
305 data into different hierarchies, or clusters within the dendrogram.

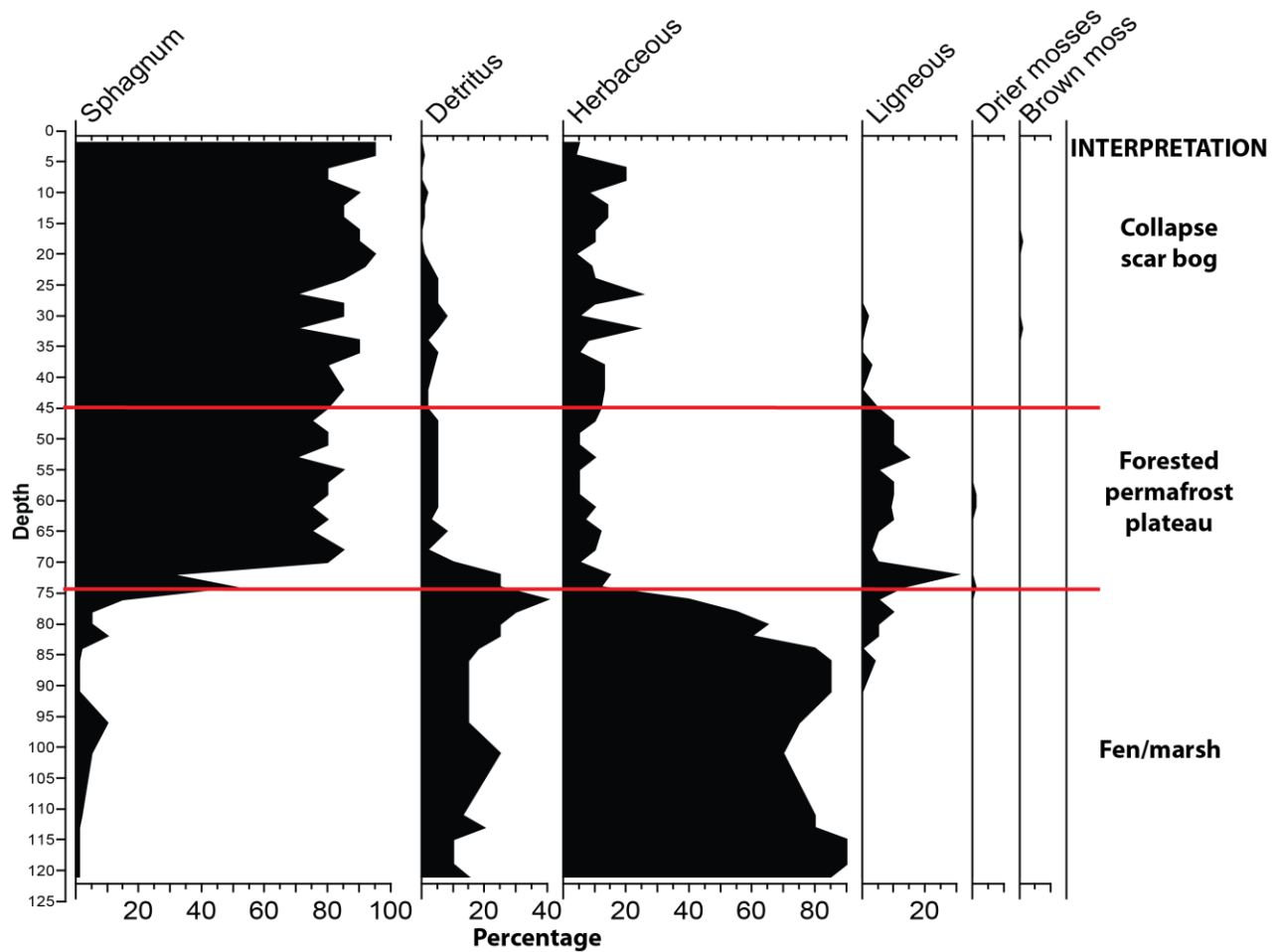
### 306 **3.0f Results**

#### 307 *3.1 <sup>210</sup>Pb and <sup>7</sup>Be results*

308 We found that <sup>210</sup>Pb age estimates for many of the soil horizons were younger than <sup>14</sup>C-based dates  
309 (Table S1). We also found movement of <sup>7</sup>Be as deep as 7 cm (Figure S1), suggesting that there was  
310 downwash of both <sup>7</sup>Be and <sup>210</sup>Pb into the soil profile. This result is supported by the fact that we also  
311 found unsupported <sup>210</sup>Pb activity as deep as 75 to 135 cm within the soil profile (Manies et al., 2021).  
312 Downwash biases the mean accumulation rate (MAR) towards higher values which, in turn, results in  
313 younger estimated ages at a specific horizon. Attempts to account for the effect of downwash on <sup>210</sup>Pb  
314 age dating using two different models was unsuccessful (Manies et al., 2016). Therefore, we did not use  
315 <sup>210</sup>Pb data in our age models, but instead only use <sup>14</sup>C measurements of macrofossils for age modeling.

#### 316 *3.2 Site history*

317 Age model results from the nine cores, all located within the 0.2 km<sup>2</sup> study area, reveal that the onset of  
318 peat formation began at the study site between -700 to 500 CE (Table 1). Sites closer to the Tanana  
319 River are younger by several hundred years (Figure S2), suggesting that, even within this site's small  
320 footprint, peat formation was influenced by the retreat of the river. Plant macrofossils indicate that peat



321

322 Figure 2. Simplified macrofossil diagram showing how changes in different amounts of material were  
 323 used to determine the transitions between stratum ecosystems. Collapse scar bogs were dominated by  
 324 bryophytic peat, while permafrost plateau forests had high levels of ligneous peat. At the base of all  
 325 cores was material dominated by herbaceous peat from the initial fen/marsh period. This diagram is for  
 326 the Young bog-4 core (BB4). Full macrofossil diagrams can be found in Figure S7.

327 is dominated by herbaceous material, typically from sedges (Cyperaceae) and ericaceous plants (Figures  
 328 2 & S7), indicating that this site was initially dominated by fen and marsh vegetation. Much of the peat  
 329 within the fen-marsh stratum was classified as plant detritus, indicating this peat's C is highly processed.  
 330 This marsh/fen stratum was present at the base of all cores.

331 Above the marsh/fen stratum, all cores transitioned to plant macrofossils dominated by ligneous  
 332 peat (e.g., black spruce roots or needles, ericaceous shrub roots, leaves; Figures 2 & S7). The transition  
 333 between herbaceous and ligneous peat indicates when permafrost first aggraded at the site, approx.

334 1450 - 1770 CE. Cores from the collapse-scar bog also had a surficial stratum dominated by bryophytic  
 335 peat (*Sphagnum*-dominated, with occasional appearance of brown mosses and Cyperaceae) consistent  
 336 with permafrost thaw (Figures 2 & S7). Age models suggest that permafrost thaw began between 1874 –  
 337 1963 CE (Table 1). Because cores were taken in different locations within each feature (e.g., center and  
 338 edge) we can use these data to understand how these features expanded. Thaw dates suggest that small  
 339 features initially formed and that these features expanded in the past decades (Figure S3). To  
 340 understand more about this expansion, we examined images of the area from 1969 (Declassified  
 341 CORONA Satellite Imagery) and 1994 (air photos). These images confirm that features were mostly  
 342 formed by 1969 with slight expansion up to 1994 and present day.

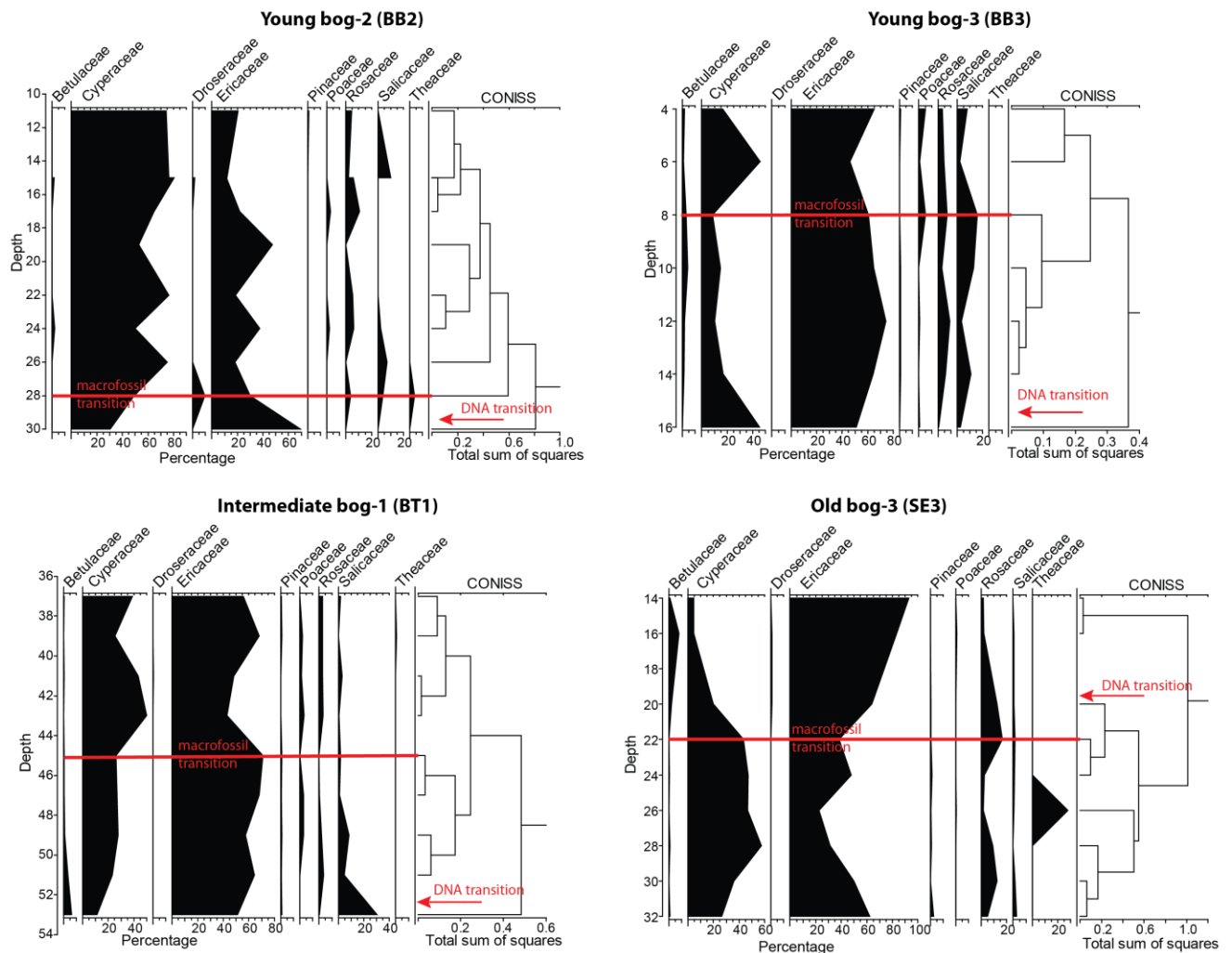
### 343 3.3 Macrofossil – DNA comparison

344 Similar to macrofossils, the relative abundance of the chloroplast nucleic acid biomarker (*trnL*) showed  
 345 changes in vegetation composition with depth for all cores. Some of the main vegetation classes found  
 346 in the DNA data align with macrofossils found in relatively high abundance (for example, Betulaceae,  
 347 Cyperaceae, and Ericaceae). However, even though mosses, especially *Sphagnum* spp., were often a  
 348 large component of the macrofossil data, none of the moss species identified in the macrofossils were

Site	Core	Peat initiation (CE)	Age of Permafrost aggradation (CE)	Age of Permafrost thaw (CE)
Young bog	BZBB 2	-110 (-226 – 34)	1447 (1285 – 1577)	1933 (1825 – 1971)
	BZBB 3	-203 (-607 – 118)	1469 (1139 – 1671)	1999 (1983 – 2011)
	BZBB 4	-468 (-668 – -376)	1710 (1676 – 1767)	1936 (1868 – 1976)
Intermediate bog	BZBT 1	42 (-50 – 196)	1601 (1475 – 1766)	1954 (1752 – 1981)
	BZBT 9	494 (144 – 952)	1769 (1689 – 1855)	1976 (1969 – 1986)
Old bog	BZSE 3	-49 (-514 – 408)	1563 (1402 – 1756)	1994 (1981 – 2004)
	BZSE 4	-156 (-195 – -100)	1710 (1541 – 1746)	1874 (1705 – 1846)
Permafrost plateau	BZPP 11	84 (-478 – 464)	1623 (1473 – 1769)	--
	BZGC 11	-711 (-910 – -508)	1675 (1464 - 1808)	--

349 **Table 1.** Estimates of ages for peat formation (aka landform age), permafrost aggradation, and  
 350 permafrost thaw. Age estimates are based on Bacon age model results (Figure S8) using radiocarbon  
 351 data (Table S2) for the depths at which transitions between stratums were noted using macrofossils  
 352 (Figure S7).

353 identified in the extracted and sequenced DNA. Missing vegetation in DNA analyses, mostly arboreal and  
 354 *Sphagnum* species, has also been noted by others (Birks & Birks, 2016; Zimmermann et al., 2017). These  
 355 missing taxa may be due to issues of primer bias, DNA degradation, plant protection of DNA, database  
 356 representation, and/or DNA extraction efficiency (Parducci et al., 2015). We used the CONISS method  
 357 (Grimm, 1987), a stratigraphically constrained cluster analysis, to determine where the DNA-based data  
 358 transitioned from a forested permafrost plateau to a collapse scar bog and compared these values to  
 359 the macrofossil-based depths. Of the four cores for which we have both *trnL* DNA and morphological-



360

361 **Figure 3.** Vegetation transition analysis from peat cores using CONISS analysis of plant DNA at the family  
 362 level. The red lines indicate the depths of macrofossil-based strata transitions, while the red arrows  
 363 indicate where the CONISS analyses indicates the first break in the DNA data.

364 macrofossil data, two of the DNA dendrograms showed a first-level split into clusters at a similar depth  
 365 as the macrofossils (Figure 3, Young bog-2 and Old bog-3). In the other two cores the DNA-based depth  
 366 of transition did not match the macrofossil-based depth (Young bog-3 and Intermediate bog-1). If we  
 367 relied on the DNA-based first level split the differences in transition depths would have changed the  
 368 estimated C stocks in the thawed bog stratum -3.2 to 0.5 kg m<sup>-2</sup>, which is up to a 30 % difference.  
 369 Because the main identifier of collapse-scar bog peat is the presence of moss species like *Sphagnum*  
 370 *angustifolium* and *Sphagnum riparium*, we chose to only use the macrofossil approach to determine  
 371 stratigraphic boundaries.

### 372 3.4 C stocks and loss with thaw

373 Total peat C stocks (to mineral soil) ranged from 24.6 – 93.1 kg m<sup>-2</sup>, but this C was divided  
 374 between 2-3 stratum, depending on location of the core. Stocks of C of the fen/marsh stratum ranged  
 375 between 16 and 42 kg C m<sup>-2</sup>, with one core having 80 kg C m<sup>-2</sup> (Table 2). There was a moderate  
 376 logarithmic relationship between the amount of C within the fen/marsh stratum and the number of  
 377 years the core was a fen/marsh ( $a= 2.27$ ,  $b=-14.65$ , goodness of fit = 0.49, Figure S4). C stocks for the  
 378 permafrost forest stratum ranged between 4.6 and 13.0 kg C m<sup>-2</sup> (Table 2) and also had a moderate

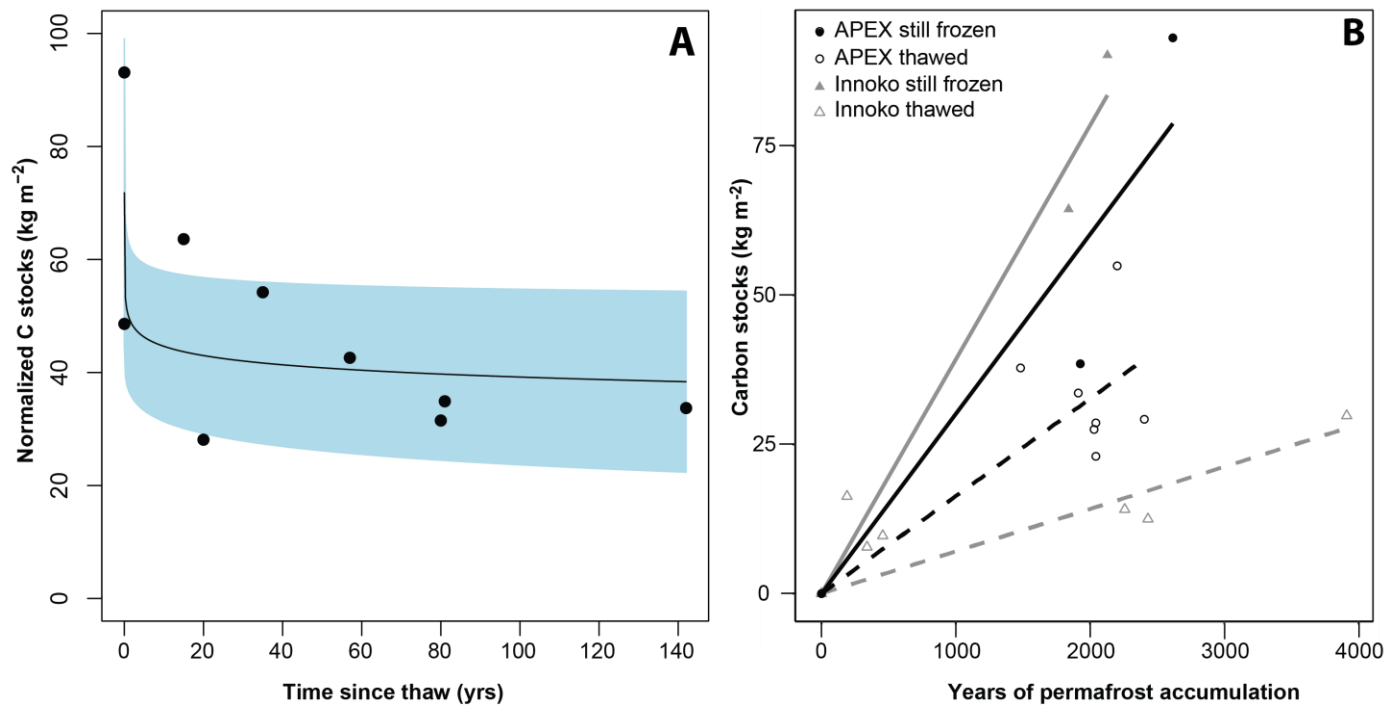
Site	Core	Carbon stocks (kg C m <sup>-2</sup> ) in peat			
		fen/marsh	forested permafrost plateau	collapse-scar bog	Total stocks
Young bog	BZBB 2	16.4	12.2	3.0	31.7
	BZBB 3	42.4	12.6	0.7	55.6
	BZBB 4	22.2	7.0	9.7	38.9
Intermediate bog	BZBT 1	29.0	4.6	7.4	41.0
	BZBT 9	26.4	11.4	4.9	42.7
Old bog	BZSE 3	17.5	5.5	1.5	24.6
	BZSE 4	22.0	5.5	10.7	38.2
Permafrost plateau	BZPP 11	26.5	12.0	--	38.5
	BZGC 11	80.1	13.0	--	93.1

379 **Table 2.** C storage (kg m<sup>-2</sup>) for the three different core strata (fen/marsh, forested permafrost plateau,  
 380 and collapse-scar bog peat) representing the three different periods this site has experienced (post-  
 381 floodplain vegetation, permafrost aggradation, and post-thaw). The permafrost plateau does not have  
 382 bog peat because these areas still contain permafrost.

383 logarithmic relationship between C stocks and number of years with permafrost ( $a=0.7575$ ,  $b=4.96$ ,  
384 goodness of fit = 0.69, Figure S4).

385 When C loss due to thaw was examined using normalized stocks, we found a loss of C in the  
386 century following permafrost thaw of 34%, or  $20 \text{ kg m}^{-2}$ , with a range of 8 - 60% (95% confidence  
387 intervals: Figure 4A). When using the slope method to compare C stocks of cores from the permafrost  
388 plateau, where the peat remains frozen, to the non-bog peat for cores where permafrost has thawed  
389 (Figure 4B), we find a 46% decrease in C (Figure 4B), which, if peat has accumulated for 2000 years,

390



391

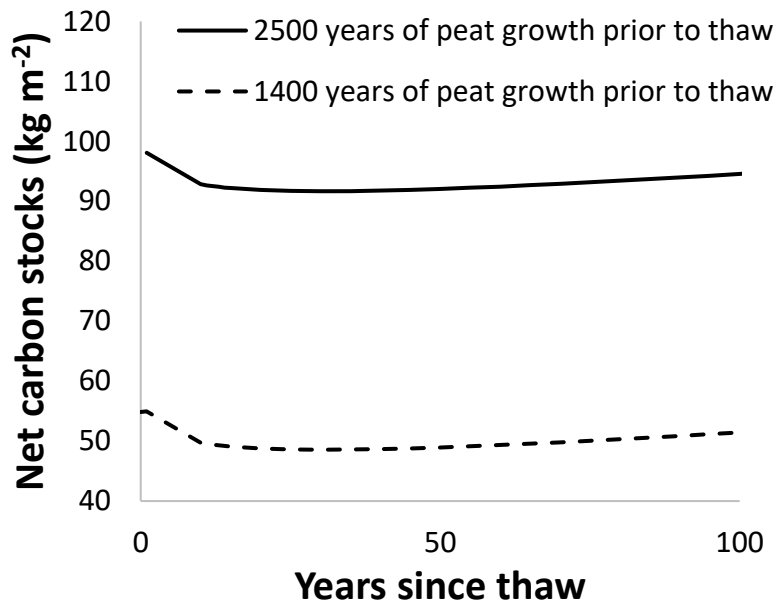
392 **Figure 4.** Estimating carbon losses from APEX permafrost using two methods. A) The Normalized C  
393 method, where C stocks were normalized to the oldest core and then plotted against the number of years  
394 each core has been thawed (see methods). This method shows a 34% loss of C with time. B) The linear  
395 method comparing stocks between still frozen peat (solid lines) and thawed peat (dashed lines) for both  
396 the APEX site (black, this study) and Innoko, AK (gray, Jones et al., 2017). With C loss, the slope of the line  
397 representing thawed cores (dashed line) will have a lower slope than the slope of the line where the  
398 cores still contain permafrost (solid line). Using this method AEPX C losses are estimated at 46% of the  
399 existing stocks, but lower than losses of C found for Innoko.

400 means a C loss of 27 kg C m<sup>-2</sup>. If we compare results of the linear method for APEX to those of Innoko,  
401 AK, which is of a similar age but formed permafrost syngenetically with peat accumulation (Jones et al.,  
402 2017; Figure 4B), we observe both lower C accumulation in APEX than Innoko as well as smaller losses.  
403 Thus, C losses (kg m<sup>-2</sup>) at APEX are over 50% less than found at Innoko. The slope method has two  
404 assumptions: 1) peat C at initiation is zero, and 2) peat accumulates linearly with time. A linear  
405 relationship may not be a true representation of peat accumulation but the short time span between  
406 permafrost initiation and thaw at APEX precludes us from determining the nature of this relationship  
407 (i.e., logarithmic, exponential, etc.) Stocks of post-thaw collapse-scar bog peat ranged between 0.7 and  
408 10.7 kgC m<sup>-2</sup>. While we found a moderate logarithmic relationship between the amount of C and the  
409 number of years for which the core was a collapse-scar bog (goodness of fit = 0.60, Figure S4), the initial  
410 accumulation rates for this model were unreasonable (>3 kg m<sup>-2</sup> yr<sup>-1</sup>). Therefore, a polynomial  
411 relationship appears to better represent our data (intercept = -0.1551, x = 0.1996, x<sup>2</sup> = -0.0003, adjusted  
412 r<sup>2</sup> = 0.64).

413 We calculated net C gains/losses by summing C gains with post-thaw moss peat growth (Figure  
414 S4) with losses with thaw, using logarithmic relationships for permafrost C loss with thaw (Figure 4A).  
415 Results suggest that the site experienced net C losses in the first 10 years following thaw, but post-thaw  
416 peat accumulation resulted in net C gains thereafter (Figure 5). Carbon stocks reached their pre-thaw  
417 levels within 150 years, regardless of the number of years we model for pre-thaw peat accumulation  
418 (Figure 5).

### 419 *3.5 C:N ratio comparison between APEX and Innoko*

420 C:N ratios can be indicative of how decomposed plant residues are, as C:N ratios typically decline during  
421 the decomposition processes, especially when examined with a vegetation type or ecosystem type



422

423 **Figure 5.** Net C stocks, modeled as inputs from bog C and losses due to permafrost thaw for two time  
 424 periods, which represent the upper and lower estimates of that at which peat initiated.

425 (Treat et al., 2016). Syngenetic permafrost would, therefore, be expected to have higher C:N ratios than  
 426 quasi-syngenetic or epigenetic permafrost because in syngenetic permafrost the plant tissue was  
 427 entrained in permafrost before much decomposition could occur. In contrast, quasi-syngenetic  
 428 permafrost and epigenetic permafrost forms after peat formation, incorporating peat that  
 429 has already been exposed to microbial processing. To determine how well nutrient concentrations work  
 430 in this capacity we compared the C:N ratios, as well as concentrations of C and N, from APEX, which  
 431 contains quasi-syngenetic permafrost, to Alaskan sites with syngenetic permafrost peat (Innoko and  
 432 Koyukuk NWR; Jones et al., 2017). An ANOVA (*av* command; R Core Team, 2017) was used to compare  
 433 these values between sites and among organic soil horizons. The soil horizons (fibric, mesic, and humic)  
 434 (Manies et al., 2020) are based on visual quantifications of the degree of decomposition within the soil  
 435 sample, not a detailed macrofossil analysis. We found that permafrost type ( $p < 0.001$ ,  $F = 62.16$ ), but  
 436 not horizon code nor a permafrost by horizon code interaction, had a significant effect on C:N ratios.  
 437 Subsequent statistical comparison of C found similar results, with permafrost type being the only

438 significant factor ( $p < 0.001$ ,  $F = 88.3$ ), with epigenetic permafrost having lower C concentrations than  
439 syngenetic permafrost (31.3 versus 41.2% C, respectively, Figure S6). Permafrost type was also a  
440 significant factor for N concentrations ( $p < 0.001$ ,  $F = 19.0$ ), with epigenetic permafrost having higher N  
441 than syngenetic permafrost (1.6 versus 1.3 % N, respectively, Figure S6). In addition, there was a  
442 permafrost by horizon interaction ( $p < 0.03$ ,  $F = 4.7$ ), with mesic epigenetic permafrost having higher N  
443 concentration than humic epigenetic permafrost (1.8 versus 1.3 % N, respectively, Figure S6).

## 444 **4.0 Discussion**

### 445 *4.1 Site history*

446 The Alaska Peatland Experiment (APEX) research site experienced permafrost thaw within the last  
447 half century, resulting in the formation of multiple thermokarst bogs of different ages. The  
448 paleoecological history of the site has been influenced local flooding due to its proximity to the Tanana  
449 River. Large floods occurred along the Tanana River from -1050 to -50 CE (Mason & Begét, 1991), which  
450 coincides with the timing of peat initiation at this site (-710 to -500 CE; Figure S2), suggesting that a  
451 combination of a decrease in river flooding and a movement of the river away from the study site  
452 allowed for peat initiation to begin. Variability in peat initiation ages is likely related to differences in  
453 local microtopography and hydrology as the Tanana River moved away from the site, with locations to  
454 the north and the west of the site (e.g., BZGC11) initiating before areas to the south or east (Figure S2).  
455 Macrofossils reveal that these sites existed as permafrost-free fens until permafrost aggraded between  
456 1450 – 1775 CE (Table 1), which corresponds to one of the maxima of the Little Ice Age (LIA; Miller et al.,  
457 2012). This timing is also consistent with broader scale Holocene climatic changes that resulted in a  
458 general increase in the aggradation of permafrost in northern peatlands ~1000 years ago, culminating  
459 during the LIA (Treat & Jones, 2018).

460 We were surprised to find that the age of permafrost thaw did not correlate to thaw feature size.  
461 While thaw in the 'old bog' appears to have begun thawing decades before the two younger bogs, the  
462 features we called 'young' and 'intermediate' appear to have begun thawing around the same time  
463 (Table 1). What differs between these two bogs is how fast the feature expanded; the young bog  
464 remained small for decades and only recently has begun expanding, while the intermediate bog appears  
465 to have been expanding since thaw began in the 1950's.

466 Several reasons could explain the difference in how fast these bogs expanded. One factor could be  
467 differences in ice content, as permafrost with high ice content is at greater risk of thaw resulting in  
468 thermokarst (Olefeldt et al., 2016; Shur & Jorgenson, 2007). High ice content soil is often associated with  
469 fine-grained surficial deposits (Jorgenson & Osterkamp, 2005). The proximity of the APEX site to the  
470 Tanana River suggests that, as the river meandered away, areas that were located in low-energy  
471 environments could have received higher amounts fine-grained sediment and, thus, could have higher  
472 mineral soil ice content. These localized areas of greater ground ice content could cause differential  
473 rates of bog expansion upon thaw. To investigate this hypothesis, we examined the volumetric water  
474 content (VWC), which would be higher in soils with more ice, of mineral soils below the active layer for  
475 cores taken around the site. The VWC content of cores taken near to the young thaw feature was lower  
476 ( $p = 0.006$ , Figure S5) than cores taken near the intermediate thaw feature, which experienced much  
477 quicker expansion (VWC  $57.3 \pm 11.4$  % versus  $64.6 \pm 15.6$  %, respectively, mean  $\pm$  s.d.).

478 Another factor that could have impacted the rates at which the young and intermediate bogs  
479 expanded is soil temperature. Data from Waldrop et al. (2021) show that in September 2015 the deep  
480 peat at the intermediate bog was warmer the deep peat at the young bog. Neumann et al. (2019)  
481 demonstrated that the temperature of rain and any resulting subsurface flow can impact deep soil  
482 temperatures, especially at bog edges. Therefore, if the intermediate bog received more water inputs  
483 from the surrounding forested permafrost plateau than the young bog these additional inputs could

484 have resulted in warmer peat temperatures, which in turn could have expanded the intermediate bog  
485 faster than the young bog. Macrofossils support this hypothesis, as cores from the intermediate bog  
486 show the presence of brown mosses, which suggests more mineral/nutrient input, such as through  
487 groundwater or overland flow. These mosses were not found in the cores from the young bog.

488 External factors, such as wildfire and solar based thermal inputs could also explain the expansion  
489 differences between the young and intermediate bogs. The only core for which charcoal appears in  
490 horizons dated from the past two centuries (when thaw began in this area) is Young bog-4. Therefore,  
491 although it is possible that fire played a role in advancing permafrost thaw at these bogs, it is not likely.  
492 Although the features are surrounded by similar vegetation, local differences in shading at the areas of  
493 initial thaw between the young and intermediate bog could have impacted thaw rates. However, ice  
494 content and/or water inputs likely played a larger role in these different rates of growth.

#### 495 4.2 Plant DNA-based stratigraphy

496 Many studies have demonstrated that DNA-based analyses, such as sequencing of the *trnL*  
497 chloroplast intron, can be used to understand long-term paleoecological changes in vegetation similar to  
498 macrofossils (i.e. thousands of years; Parducci et al., 2017; Parducci et al., 2015; Zimmermann et al.,  
499 2017). Our DNA-based reconstruction identified fewer taxa than identified by the macrofossil analysis,  
500 as is consistent with the literature (see Figure 2 of Parducci et al., 2015). Changes in moss species is a  
501 key indicator of thaw, both in the field and in macrofossil analyses, but was mostly absent from our DNA  
502 analyses. We identified three potential reasons for this under-representation of bryophytes in the  
503 sequence-based data set. Firstly, the primers used targeted the P6-loop of the chloroplast *trnL* (UAA)  
504 intron, which is a universal, short, plant-specific biomarker. Although these same primers have been  
505 shown to successfully amplify and identify *Sphagnum* spp. from Arctic sediment cores, *Sphagnum* are  
506 not the main target of these primers and, therefore, amplification may be biased against inclusion in a  
507 *trnL* sequence-based dataset (Alsos et al., 2016; Zimmermann et al., 2017). Secondly, the identification

508 of sequences species relies on the completeness of the reference database. We used European  
509 arctic/vascular and bryophyte databases, because as yet no Northern American arctic/boreal plant  
510 database with the chloroplast *trnL* (UAA) intron exists, which also could have cause bias against  
511 identification of locally adapted *Sphagnum* spp. Finally, when *Sphagnum* biomass is buried cell lysis and  
512 the presence of secondary metabolites may increase the rate of DNA degradation (Xie & Lou, 2009). We  
513 believe with further improvement this method could be more useful for palaeoecological studies of  
514 Alaskan flora and, potentially, though inclusion of *Sphagnum* specific primers, useful for identification of  
515 vegetation transitions across broad time scales.

516           We were interested in knowing if these DNA based methods could be used to mark finer-scale  
517 (decadal) transitions between vegetation, such as when permafrost thawed and forested peat plateaus  
518 transitioned into inundated wetlands, as this determination using macrofossil data is a time- and  
519 training-intensive process. Identification of stratigraphic transitions between bogs and forest peat  
520 plateaus using the *trnL* amplicon only matched (within 2 cm) morphological identification-based  
521 transitions in two of the four cores we examined. We should note that due to time and sample  
522 constraints, we only conducted DNA-based analyses on ~20-cm sections of each core, focused on the  
523 area where macrofossil data indicated a vegetation community shift occurred. Even considering this  
524 constraint, because the *trnL* vegetation reconstructions using the methods detailed herein do not  
525 consistently match macrofossil results we feel they are better used as a complementary tool, one that  
526 could be used as a ‘first pass’ in paleoecological studies, in conjunction with morphological macrofossil  
527 analyses, or when examining vegetation shifts across an entire core, representing tens of thousands of  
528 years of ecosystem change.

#### 529 *4.3 Estimating C losses in millennial aged permafrost*

530           The magnitude of post-thaw C loss of lowland peatlands remains a matter of debate. While  
531 some studies have found large permafrost C losses due to permafrost thaw (Jones et al., 2017;

532 O'Donnell et al., 2012), others show little to no loss, such that any losses can be relatively quickly  
533 recouped with post-thaw peat accumulation (Cooper et al., 2017; Estop-Aragonés et al., 2018a; Estop-  
534 Aragonés et al., 2018b; Heffernan et al., 2020). We found evidence that between 34 – 46% of the C  
535 available at APEX was lost due to thaw (Figure 4). However, the scatter in our dataset was relatively  
536 high, suggesting additional replicate cores and/or a chronosequence spanning a greater period of time  
537 would help constrain these values. We attribute the high scatter in the APEX dataset to natural  
538 landscape variability, the clustering of thaw ages within a few decades of each other, and radiocarbon  
539 calibration uncertainty associated with the timing of thaw coinciding with nuclear weapons testing.  
540 Additional sources of uncertainty include the fact that some ages were derived from the age model, due  
541 to lack of  $^{14}\text{C}$  dates at the depth of transition, and the potential of mixing of macrofossil assemblages,  
542 which can happen due to edge slumping. Nonetheless, our data suggests that 20 - 27 kg C m<sup>-2</sup> was lost  
543 due to thaw at APEX (normalized versus linear method, respectively). These values are greater than the  
544 9 kg C m<sup>-2</sup> of losses found by Heffernan et al. (2020), but less than the 35 – 45 kg C m<sup>-2</sup> of losses found by  
545 Jones et al. (2017). When comparing the APEX data with the data from Innoko, Alaska (Jones et al.,  
546 2017), which used similar methods for estimating C loss, we show that the Innoko permafrost plateaus  
547 both gained more C prior to thaw and lost more carbon following thaw compared to APEX (Figure 4B).  
548 We compared these two sites because peat initiated around the same time (Table 3; Figure 4B). We  
549 believe the main difference between these two sites is that Innoko contains syngenetic permafrost,  
550 where peat and permafrost accumulation happened simultaneously. In contrast, the permafrost at APEX  
551 was classified as quasi-syngenetic permafrost, a form of epigenetic permafrost. Quasi-syngenetic  
552 permafrost forms when the permafrost grows upward, like syngenetic permafrost, but incorporates  
553 already existing peat/sediments (Kanevskiy, 2003). Therefore, the permafrost at APEX aggraded  
554 following peat initiation and has only existed for several hundred years.

555 Differences in permafrost aggradation processes impacts how decomposed peat is, and,  
556 therefore, its chemical composition prior to its incorporation into permafrost (Treat et al., 2014).  
557 Because syngenetic permafrost is formed when permafrost aggradation and peat accumulation occur in  
558 tandem, syngenetic peat is less decomposed and, therefore, likely more susceptible to decomposition  
559 upon thaw. In contrast, epigenetic and quasi-epigenetic permafrost are formed with previously  
560 deposited sediments/peats, which have already been subject to microbial turnover and, therefore, likely  
561 decay more slowly upon thaw. Evidence of high pre-permafrost C processing at APEX is evidenced by an  
562 abundance of detrital peat in the fen/marsh stratum (Figures 2 & S6), suggesting that the most labile  
563 fraction was processed prior to permafrost aggradation, rendering it less prone to further  
564 decomposition upon thaw. This result lies in contrast to the syngenetic permafrost peat plateaus at  
565 Innoko and Koyukuk NWR (Alaska), whose peat plateaus contained well-preserved peat in the  
566 permafrost (Jones et al., 2017; O'Donnell et al., 2012), subjecting it to rapid decomposition upon thaw.

567 Age factors, such as number of years a site has accumulated peat and had permafrost aggrading,  
568 also impact the amount of peat that has accumulated and, thus, the amount of C that can be lost due to  
569 thaw. Therefore, we compared these age factors, along with permafrost type, for studies that had  
570 examined C loss with permafrost thaw (Table 3). There was no consistent pattern between amount of C  
571 lost and landform age. There was also no consistent pattern in number of years for which a site had  
572 permafrost and magnitude of C loss. However, there was a trend with higher losses coming from sites  
573 with syngenetic permafrost and smaller losses coming from sites with epigenetic or quasi-syngenetic  
574 permafrost, suggesting that type of permafrost is an important factor in determining the relative  
575 amount of C loss due to thaw. Unfortunately, the one study site that contained both syngenetic and  
576 epigenetic permafrost (Estop-Aragonés et al., 2018a) used a different methodology to look at C loss (<sup>14</sup>C-  
577 based methods), precluding an examination into how the presence of both types of permafrost might  
578 influence C loss. We also found that, as in other studies (e.g., Heffernan et al., 2020), if losses are

579 **Table 3.** Comparison of common factors for studies that have seen minimal versus large C losses with permafrost thaw. While landform age as  
 580 well as the number of years the forest peat stratum was frozen and has been thaw all play a role in C loss, another important factor for  
 581 determining if there will be small versus large losses appears to be permafrost type. Syngenetic permafrost, which consists of relatively  
 582 unprocessed peat, tends to experience larger C losses, while permafrost that formed after peat formed (epigenetic and quasi-syngenetic), so that  
 583 the peat has previously been processed, appear to experience small losses.

Relative amount of C loss	Permafrost type	Landform Initiation	Number of years permafrost present	Number of years permafrost thawed (approx.)	General Location	Method
smaller	epigenetic (processed peat)	-450 – 550 CE (2400 – 1400 BP)	200-400	20 - 100	Fairbanks Alaska <sup>a</sup>	chronosequence
smaller	epigenetic (processed peat)	-6550 CE (8500 BP)	1800	30 – 200	AB, Canada <sup>b, c</sup>	chronosequence, <sup>14</sup> C
smaller	syngenetic and epigenetic (unprocessed and processed peat)	-5550 – -4650 CE (6600 – 7500 BP)	Unknown	20 - 130	NWT, Canada <sup>d</sup>	<sup>14</sup> C
larger	syngenetic (unprocessed peat)	-6050 – -8050 CE (8000 – 1000 BP)	8,000-10,000	30 - 1215	Koyukuk, Alaska <sup>e, f</sup>	chronosequence
larger	syngenetic (unprocessed peat)	-1050 – -50 CE (2000 – 3000 BP)	2,000-3,000	20 - 400	Innoko, Alaska <sup>f</sup>	chronosequence

584 <sup>a</sup>This study

585 <sup>b</sup>Heffernan et al. (2020)

586 <sup>c</sup>Estop-Aragónés et al. (2018b)

587 <sup>d</sup>Estop-Aragones et al. (2018a), Wolfe et al. (2017)

588 <sup>e</sup>O'Donnell et al. (2012)

589 <sup>f</sup>Jones et al. (2017)

590 relatively small, they are often recuperated relatively quickly (decades to centuries versus millennia)  
591 post-thaw.

592           The role that type of permafrost plays suggests that better understanding of the spatial  
593 distribution of syngenetic and epigenetic permafrost could help constrain the landscape-scale  
594 magnitude of C loss from permafrost thaw in boreal peat plateaus. While the spatial extent of  
595 syngenetic versus epigenetic permafrost is not well documented, analysis of circumpolar peat cores  
596 revealed patterns of permafrost aggradation timing relative to peatland age, suggesting that the  
597 majority of permafrost peatlands aggraded permafrost epigenetically within the late Holocene and as  
598 recently as the Little Ice Age (Treat and Jones, 2018). We must also recognize that soils can reflect  
599 complex sequences of different types of permafrost formation, with multiple types of permafrost found  
600 within the same location (Kanevskiy et al., 2014; Wolfe et al., 2014).

601           Due to the lack of permafrost type maps and the possibility of both syngenetic and epigenetic  
602 permafrost within a single core, other indicators need to be used to determine if thawing peat is  
603 susceptible to small or large C losses. Our results suggesting that C:N ratios would be a good first-order  
604 indicator of permafrost type align with the results others (Sannel & Kuhry, 2009; Schädel et al., 2014;  
605 Treat et al., 2016) In addition, C:N data are more accessible in comparison to macrofossil analyses,  
606 which require training and are time intensive. The differences in C:N ratios between permafrost types is  
607 driven more by differences in C concentration (epigenetic = 31.3% versus syngenetic = 41.2%; Figure S6)  
608 than N concentration (epigenetic = 1.6% versus syngenetic = 1.3%; Figure S6). Epigenetic permafrost  
609 also has greater variability in C concentrations than syngenetic permafrost. Lower C concentrations for  
610 epigenetic permafrost are representative of the fact that its C has experienced more decomposition  
611 (Schädel et al., 2014) than syngenetic permafrost.

612 **5.0 Conclusions**

613 We found that for the APEX site, located near the Tanana River of Interior Alaska, the timing of  
614 peat initiation was impacted by proximity to old river channels. Initially these sites were dominated by  
615 sedges and woody vegetation, consistent with rich fens that accumulated peat in the absence of  
616 permafrost. Permafrost aggraded at this site at the end of the Little Ice Age, consistent with  
617 observations of other permafrost peatlands in the discontinuous permafrost zone in Alaska. In the last  
618 century, permafrost began to degrade in places, transitioning some of the forested peat plateaus in this  
619 area into collapse-scar bogs. We found variable rates of bog expansion for the three different features  
620 studied herein and hypothesize that these differences are related to within-site differences such as  
621 ground ice content and the amount of overland flow received.

622 Using two different methods, we found smaller C losses post thaw ( $20 - 34 \text{ kg C m}^{-2}$ ) compared  
623 to other Alaskan locations. Based on a comparison of our results to other studies in the literature that  
624 also examined changes in permafrost C upon thaw, we conclude that in addition to landform age and  
625 length of time as permafrost, the permafrost aggradation process influences C loss with thaw. Areas  
626 where permafrost aggrades after peat formation (i.e., epigenetic) will experience less C loss with thaw,  
627 while sites that have syngenetic permafrost could experience large losses of C with thaw. Therefore,  
628 future research into changes in C loss with thaw should include determining the relative coverage of  
629 these permafrost types within the boreal region. Where this information is not known C:N ratios can be  
630 used to indicate the degree of processing of the peat, informing estimates of the degree of C loss with  
631 thaw.

632 **Data Availability**

633 Data used in this study are available from Manies et al. (2021; <https://doi.org/10.5066/XXXXXXXX>).

634 [Note to reviewers: This data release is currently under internal USGS review, so the doi number has yet  
635 to be assigned.]

636 **Acknowledgements**

637 We would like to acknowledge Yen Le for her help with the molecular analyses and Jack McFarland for  
638 advice and help efficiently sampling and subsampling these cores. Thanks to Mikhail Kanevskiy for his  
639 assistance in determining the type of permafrost found at APEX. We also would like to acknowledge the  
640 assistance of the Fairbanks USGS office and the Bonanza Creek LTER, without which this work would not  
641 be possible. This work was funded by the USGS Climate and Land Use Change Program. Any use of trade,  
642 firm, or product names is for descriptive purposes only and does not imply endorsement by the U.S.  
643 Government.

644 **References Cited**

- 645
- 646 Alsos, I. G., Sjögren, P., Edwards, M. E., Landvik, J. Y., Gielly, L., Forwick, M., et al. (2016). Sedimentary  
647 ancient DNA from Lake Skartjørna, Svalbard: Assessing the resilience of arctic flora to Holocene  
648 climate change. *The Holocene*, 26(4), 627-642.
- 649 Birks, H. J. B., & Birks, H. H. (2016). How have studies of ancient DNA from sediments contributed to the  
650 reconstruction of Quaternary floras? *New Phytologist*, 209(2), 499-506.
- 651 Blaauw, M., & Christen, J. A. (2011). Flexible paleoclimate age-depth models using an autoregressive  
652 gamma process. *Bayesian Anal.*, 6(3), 457-474.
- 653 Boyer, F., Mercier, C., Bonin, A., Le Bras, Y., Taberlet, P., & Coissac, E. (2016a). obitools: a unix-inspired  
654 software package for DNA metabarcoding. *Mol Ecol Resour*, 16(1), 176-182.
- 655 Boyer, F., Mercier, C., Bonin, A., Le Bras, Y., Taberlet, P., & Coissac, E. (2016b). obitools: a unix-inspired  
656 software package for DNA metabarcoding. *Molecular Ecology Resources*, 16(1), 176-182.
- 657 Brown, J., Ferrians Jr, O. J., Heginbottom, J. A., & Melnikov, E. S. (1997). *Circum-Arctic map of permafrost*  
658 *and ground-ice conditions* Circum-Pacific Map 45.
- 659 Brown, J., & Kreig, R. A. (1983, July 18-22). *Guidebook to permafrost and related features along the*  
660 *Elliott and Dalton highways, Fox to Prudhoe Bay, Alaska*. Paper presented at the Fourth  
661 International Conference on Permafrost, University of Alaska, Fairbanks, Alaska.
- 662 Cooper, M. D. A., Estop-Aragonés, C., Fisher, J. P., Thierry, A., Garnett, M. H., Charman, D. J., et al.  
663 (2017). Limited contribution of permafrost carbon to methane release from thawing peatlands.  
664 *Nature Climate Change*, 7(7), 507-511.
- 665 Estop-Aragonés, C., Cooper, M. D. A., Fisher, J. P., Thierry, A., Garnett, M. H., Charman, D. J., et al.  
666 (2018a). Limited release of previously-frozen C and increased new peat formation after thaw in  
667 permafrost peatlands. *Soil Biology and Biochemistry*, 118, 115-129.
- 668 Estop-Aragonés, C., Czimczik, C., I., Heffernan, L., Gibson, C., Walker, J., C., Xu, X., & Olefeldt, D. (2018b).  
669 Respiration of aged soil carbon during fall in permafrost peatlands enhanced by active layer  
670 deepening following wildfire but limited following thermokarst. *Environmental Research Letters*,  
671 13(8), 085002.
- 672 Euskirchen, E. S., McGuire, A. D., Chapin, F. S., Yi, S., & Thompson, C. C. (2009). Changes in vegetation in  
673 northern Alaska under scenarios of climate change, 2003-2100: implications for climate  
674 feedbacks. *Ecological Applications*, 19(4), 1022-1043. doi:10.1890/08-0806.1.
- 675 Finger, R. A., Turetsky, M. R., Kielland, K., Ruess, R. W., Mack, M. C., & Euskirchen, E. S. (2016). Effects of  
676 permafrost thaw on nitrogen availability and plant-soil interactions in a boreal Alaskan lowland.  
677 *Journal of Ecology*, 104(6), 1542-1554.
- 678 Gibson, C., Estop-Aragonés, C., Flannigan, M. D., Thompson, D., & Olefeldt, D. (2019). Increased deep  
679 soil respiration detected despite reduced overall respiration in permafrost peat plateaus  
680 following wildfire. *Environmental Research Letters*, 14.
- 681 Greenwell, B. M., & Schubert Kabban, C. M. (2014). investr: An R Packages for Inverse Estimation. *The R*  
682 *Journal*, 6, 90-100.
- 683 Grimm, E. C. (1987). CONISS: a FORTRAN 77 program for stratigraphically constrained cluster analysis by  
684 the method of incremental sum of squares. *Computers & Geosciences*, 13(1), 13-35.
- 685 Harden, J. W., Koven, C. D., Ping, C. L., McGuire, A. D., Camill, P., Jorgenson, M. T., et al. (2012). Field  
686 information links permafrost carbon to physical vulnerabilities of thawing. *Geophysical Research*  
687 *Letters*, 39(15), L15704.
- 688 Heffernan, L., Estop-Aragonés, C., Knorr, K.-H., Talbot, J., & Olefeldt, D. (2020). Long-term impacts of  
689 permafrost thaw on carbon storage in peatlands: deep losses offset by surficial accumulation.  
690 *Journal of Geophysical Research: Biogeosciences*, n/a(n/a), e2019JG005501.

691 Hinzman, L. D., Viereck, L. A., Adams, P. C., Romanovksy, v., & Yoshikawa, K. (2006). Climate and  
692 permafrost dynamics of the Alaskan boreal forest. In F. S. Chapin, III, M. W. Oswood, K. Van  
693 Cleve, L. A. Viereck, & D. Verbyla (Eds.), *Alaska's Changing Boreal Forest* (pp. 39-61). Oxford,  
694 United Kingdom: Oxford University Press.

695 Hugelius, G., Loisel, J., Chadburn, S., Jackson, R. B., Jones, M., MacDonald, G., et al. (2020). Large stocks  
696 of peatland carbon and nitrogen are vulnerable to permafrost thaw. *Proceedings of the National  
697 Academy of Sciences*, 201916387.

698 Jackson, R. B., Lajtha, K., Crow, S. E., Hugelius, G., Kramer, M. G., & Piñeiro, G. (2017). The Ecology of Soil  
699 Carbon: Pools, Vulnerabilities, and Biotic and Abiotic Controls. *Annual Review of Ecology,  
700 Evolution, and Systematics*, 48(1), 419-445.

701 Jones, M., Harden, J., O'Donnell, J., Manies, K., Jorgenson, T., Treat, C., & Ewing, S. (2017). Rapid carbon  
702 loss and slow recovery following permafrost thaw in boreal peatlands. *Global Change Biology*,  
703 23(3), 1109-1127.

704 Jorgenson, M. T., & Osterkamp, T. E. (2005). Response of boreal ecosystems to varying modes of  
705 permafrost degradation. *Canadian Journal of Forest Research*, 35(9), 2100-2111.

706 Jungqvist, G., Oni, S. K., Teutschbein, C., & Futter, M. N. (2014). Effect of Climate Change on Soil  
707 Temperature in Swedish Boreal Forests. *PLoS ONE*, 9(4).

708 Kanevskiy, M. (2003). *Cryogenetic structure of mountain slope deposits, northeast Russia*. Paper  
709 presented at the 8th International Conference on Permafrost, Zurich, Switzerland.

710 Kanevskiy, M., Jorgenson, T., Shur, Y., O'Donnell, J. A., Harden, J. W., Zhuang, Q., & Fortier, D. (2014).  
711 Cryostratigraphy and Permafrost Evolution in the Lacustrine Lowlands of West-Central Alaska.  
712 *Permafrost and Periglacial Processes*, 25(1), 14-34.

713 Leewis, M.-C., Berlemont, R., Podgorski, D. C., Srinivas, A., Zito, P., Spencer, R. G. M., et al. (2020). Life at  
714 the Frozen Limit: Microbial Carbon Metabolism Across a Late Pleistocene Permafrost  
715 Chronosequence. *Frontiers in Microbiology*, 11(1753). Original Research.

716 Malmer, N., Albinsson, C., Svensson, B. M., & Wallén, B. (2003). Interferences between Sphagnum and  
717 vascular plants: effects on plant community structure and peat formation. *Oikos*, 100(3), 469-  
718 482.

719 Manies, K., Waldrop, M., & Harden, J. (2020). Generalized models to estimate carbon and nitrogen  
720 stocks of organic soil horizons in Interior Alaska. *Earth Syst. Sci. Data*, 12(3), 1745-1757.

721 Manies, K. L., Fuller, C., & Jones, M. (2016). *Modeling Peat Ages Using <sup>7</sup>Be Data to Account for  
722 Downwash of <sup>210</sup>Pb*. Paper presented at the American Geophysical Union Fall Meeting, San  
723 Francisco, CA. <https://ui.adsabs.harvard.edu/abs/2016AGUFM.B23C0597M>

724 Manies, K. L., Fuller, C. C., Jones, M. C., Waldrop, M. P., & McGeehin, J. P. (2017). *Soil data for a  
725 thermokarst bog and the surrounding permafrost plateau forest, located at Bonanza Creek Long  
726 Term Ecological Research Site, Interior Alaska* Open-File Report 2016-1173.

727 Manies, K. L., Jones, M. C., Waldrop, M. P., Leewis, M.-C., Hoefke, K., Fuller, C., & Cornman, R. S. (2021).  
728 *Soil data and age models used to investigate the effects of permafrost thaw on carbon storage,  
729 Interior Alaska*.

730 Mason, O. K., & Begét, J. E. (1991). Late Holocene flood history of the Tanana River, Alaska, USA. *Arctic  
731 and Alpine Research*, 23(4), 392-403.

732 Miller, G. H., Geirsdóttir, Á., Zhong, Y., Larsen, D. J., Otto-Bliesner, B. L., Holland, M. M., et al. (2012).  
733 Abrupt onset of the Little Ice Age triggered by volcanism and sustained by sea-ice/ocean  
734 feedbacks. *Geophysical Research Letters*, 39(2).

735 Neumann, R. B., Moorberg, C. J., Lundquist, J. D., Turner, J. C., Waldrop, M. P., McFarland, J. W., et al.  
736 (2019). Warming effects of spring rainfall increase methane emissions from thawing permafrost.  
737 *Geophysical Research Letters*, 46, 1393-1401.

738 O'Donnell, J. A., Jorgenson, M. T., Harden, J. W., McGuire, A. D., Kanevskiy, M., & Wickland, K. P. (2012).  
739 The effects of permafrost thaw on soil hydrologic, thermal, and carbon dynamics in an Alaskan  
740 peatland. *Ecosystems*, 15, 213-229.

741 Olefeldt, D., Goswami, S., Grosse, G., Hayes, D., Hugelius, G., Kuhry, P., et al. (2016). Circumpolar  
742 distribution and carbon storage of thermokarst landscapes. *Nature Communications*, 7, 13043.  
743 Article.

744 Oliva, M., & Fritz, M. (2018). Permafrost degradation on a warmer Earth: Challenges and perspectives.  
745 *Current Opinion in Environmental Science & Health*, 5, 14-18.

746 Parducci, L., Bennett, K. D., Ficetola, G. F., Alsos, I. G., Suyama, Y., Wood, J. R., & Pedersen, M. W. (2017).  
747 Ancient plant DNA in lake sediments. *New Phytologist*, 214(3), 924-942.

748 Parducci, L., Välranta, M., Salonen, J. S., Ronkainen, T., Matetovici, I., Fontana, S. L., et al. (2015). Proxy  
749 comparison in ancient peat sediments: pollen, macrofossil and plant DNA. *Philosophical  
750 Transactions of the Royal Society B: Biological Sciences*, 370(1660), 20130382.

751 Pella, E. (1990a). Elemental organic analysis. Part 1-Historical developments. *American Laboratory*,  
752 22(2), 116-125.

753 Pella, E. (1990b). Elemental organic analyzer. Part 2-State of the art. *American Laboratory*, 22(12), 28-  
754 32.

755 R Core Team. (2017). R: A language and environment for statistical computing. Vienna, Austria: R  
756 Foundation for Statistical Computing. Retrieved from <https://www.R-project.org/>.

757 Rand, J., & Mellor, M. (1985). *Ice-coring augers for shallow depth sampling* CRREL Report 85-21.

758 Rodenhizer, H., Ledman, J., Mauritz, M., Natali, S. M., Pegoraro, E., Plaza, C., et al. (2020). Carbon Thaw  
759 Rate Doubles When Accounting for Subsidence in a Permafrost Warming Experiment. *Journal of  
760 Geophysical Research: Biogeosciences*, 125(6), e2019JG005528.

761 Sannel, A. B. K., & Kuhry, P. (2009). Holocene peat growth and decay dynamics in sub-arctic peat  
762 plateaus, west-central Canada. *Boreas: Boreas*, 38(1), 13-24. Article.

763 Schädel, C., Schuur, E. A. G., Bracho, R., Elberling, B., Knoblauch, C., Lee, H., et al. (2014). Circumpolar  
764 assessment of permafrost C quality and its vulnerability over time using long-term incubation  
765 data. *Global Change Biology*, 20(2), 641-652.

766 Schuur, E. A., McGuire, A. D., Schädel, C., Grosse, G., Harden, J. W., Hayes, D. J., et al. (2015). Climate  
767 change and the permafrost carbon feedback. *Nature*, 520(7546), 171-179.

768 Shur, Y., Jorgenson, M. T., & Kanevskiy, M. Z. (2011). Permafrost. In V. P. Singh, P. Singh, & U. K.  
769 Haritashya (Eds.), *Encyclopedia of Snow, Ice and Glaciers* (pp. 841-848). Dordrecht: Springer  
770 Netherlands.

771 Shur, Y. L., & Jorgenson, M. T. (2007). Patterns of permafrost formation and degradation in relation to  
772 climate and ecosystems. *Permafrost and Periglacial Processes*, 18(1), 7-19.

773 Soil Survey Staff. (1951). *Soil survey manual* (Vol. Handbook No. 18). Washington, D.C.: Agricultural  
774 Research Administration, United States Department of Agriculture.

775 Taberlet, P., Coissac, E., Pompanon, F., Gielly, L., Miquel, C., Valentini, A., et al. (2006). Power and  
776 limitations of the chloroplast trn L (UAA) intron for plant DNA barcoding. *Nucleic Acids Research*,  
777 35(3), e14-e14.

778 Thormann, M., Szumigalski, A., & Bayley, S. (1999). Aboveground peat and carbon accumulation  
779 potentials along a bog-fen-marsh wetland gradient in southern boreal Alberta, Canada.  
780 *Wetlands*, 19(2), 305-317.

781 Treat, C. C., & Jones, M. C. (2018). Near-surface permafrost aggradation in Northern Hemisphere  
782 peatlands shows regional and global trends during the past 6000 years. *The Holocene*, 28(6),  
783 998-1010.

784 Treat, C. C., Jones, M. C., Camill, P., Gallego-Sala, A., Garneau, M., Harden, J. W., et al. (2016). Effects of  
785 permafrost aggradation on peat properties as determined from a pan-Arctic synthesis of plant  
786 macrofossils. *Journal of Geophysical Research: Biogeosciences*, *121*(1), 78-94.

787 Treat, C. C., Wollheim, W. M., Varner, R. K., Grandy, A. S., Talbot, J., & Frolking, S. (2014). Temperature  
788 and peat type control CO<sub>2</sub> and CH<sub>4</sub> production in Alaskan permafrost peats. *Global Change*  
789 *Biology*, *20*(8), 2674–2686.

790 Turetsky, M. R., Kane, E. S., Harden, J. W., Ottmar, R. D., Manies, K. L., Hoy, E., & Kasichke, E. S. (2011).  
791 Recent acceleration of biomass burning and carbon losses in Alaskan forests and peatlands.  
792 *Nature Geosciences*, *4*, 27–31.

793 Turetsky, M. R., Manning, S. W., & Wieder, R. K. (2004). Dating Recent Peat Deposits. *Wetlands*, *24*(2),  
794 324.

795 Van Metre, P. C., & Fuller, C. C. (2009). Dual-core mass-balance approach for evaluating mercury and  
796 <sup>210</sup>Pb atmospheric fallout and focusing to lakes. *Environmental Science & Technology*, *43*, 26-32.

797 Waldo, N. B., Hunt, B. K., Fadely, E. C., Moran, J. J., & Neumann, R. B. (2019). Plant root exudates  
798 increase methane emissions through direct and indirect pathways. *Biogeochemistry*, *145*(1),  
799 213-234.

800 Waldrop, M. P., McFarland, J., Manies, K., Leewis, M. C., Blazewicz, S. J., Jones, M. C., et al. (2021).  
801 Carbon fluxes and microbial activities from boreal peatlands experiencing permafrost thaw.  
802 *Journal of Geochemical Research - Biogeosciences*.

803 Wolfe, S. A., & Morse, P. D. (2017). Lithalsa Formation and Holocene Lake-Level Recession, Great Slave  
804 Lowland, Northwest Territories. *Permafrost and Periglacial Processes*, *28*(3), 573-579.

805 Wolfe, S. A., Short, N. H., Morse, P. D., Schwarz, S. H., & Stevens, C. W. (2014). Evaluation of RADARSAT-  
806 2 DInSAR Seasonal Surface Displacement in Discontinuous Permafrost Terrain, Yellowknife,  
807 Northwest Territories, Canada. *Canadian Journal of Remote Sensing*, *40*(6), 406-422.

808 Xie, C.-F., & Lou, H.-X. (2009). Secondary Metabolites in Bryophytes: An Ecological Aspect. *Chemistry &*  
809 *Biodiversity*, *6*(3), 303-312.

810 Zhang, T., Heginbottom, J., Barry, R., & Brown, J. (2000). Further statistics on the distribution of  
811 permafrost and ground ice in the Northern Hemisphere. *Polar Geography*, *24*, 126-131.

812 Zimmermann, H. H., Raschke, E., Epp, L. S., Stoof-Leichsenring, K. R., Schwamborn, G., Schirrmeister, L.,  
813 et al. (2017). Sedimentary ancient DNA and pollen reveal the composition of plant organic  
814 matter in Late Quaternary permafrost sediments of the Buor Khaya Peninsula (north-eastern  
815 Siberia). *Biogeosciences*, *14*(3), 575-596.

816

**STAND ALONE VERSION OF TABLES AND FIGURES**

Site	Core	Peat initiation (CE)	Age of Permafrost aggradation (CE)	Age of Permafrost thaw (CE)
Young bog	BZBB 2	-110 (-226 – 34)	1447 (1285 – 1577)	1933 (1825 – 1971)
	BZBB 3	-203 (-607 – 118)	1469 (1139 – 1671)	1999 (1983 – 2011)
	BZBB 4	-468 (-668 – -376)	1710 (1676 – 1767)	1936 (1868 – 1976)
Intermediate bog	BZBT 1	42 (-50 – 196)	1601 (1475 – 1766)	1954 (1752 – 1981)
	BZBT 9	494 (144 – 952)	1769 (1689 – 1855)	1976 (1969 – 1986)
Old bog	BZSE 3	-49 (-514 – 408)	1563 (1402 – 1756)	1994 (1981 – 2004)
	BZSE 4	-156 (-195 – -100)	1710 (1541 – 1746)	1874 (1705 – 1846)
Permafrost plateau	BZPP 11	84 (-478 – 464)	1623 (1473 – 1769)	--
	BZGC 11	-711 (-910 – -508)	1675 (1464 - 1808)	--

**Table 1.** Estimates of ages for peat formation (aka landform age), permafrost aggradation, and permafrost thaw. Age estimates are based on Bacon age model results (Figure S8) using radiocarbon data (Table S2) for the depths at which transitions between stratums were noted using macrofossils (Figure S7).

Site	Core	Carbon stocks (kg C m <sup>-2</sup> ) in peat			
		fen/marsh	forested permafrost plateau	collapse-scar bog	Total stocks
Young bog	BZBB 2	16.4	12.2	3.0	31.7
	BZBB 3	42.4	12.6	0.7	55.6
	BZBB 4	22.2	7.0	9.7	38.9
Intermediate bog	BZBT 1	29.0	4.6	7.4	41.0
	BZBT 9	26.4	11.4	4.9	42.7
Old bog	BZSE 3	17.5	5.5	1.5	24.6
	BZSE 4	22.0	5.5	10.7	38.2
Permafrost plateau	BZPP 11	26.5	12.0	--	38.5
	BZGC 11	80.1	13.0	--	93.1

**Table 2.** C storage (kg m<sup>-2</sup>) for the three different core strata (fen/marsh, forested permafrost plateau, and collapse-scar bog peat) representing the three different periods this site has experienced (post-floodplain vegetation, permafrost aggradation, and post-thaw). The permafrost plateau does not have bog peat because these areas still contain permafrost.

**Table 3.** Comparison of common factors for studies that have seen minimal versus large C losses with permafrost thaw. While landform age as well as the number of years the forest peat stratum was frozen and has been thaw all play a role in C loss, another important factor for determining if there will be small versus large losses appears to be permafrost type. Syngenetic permafrost, which consists of relatively unprocessed peat, tends to experience larger C losses, while permafrost that formed after peat formed (epigenetic and quasi-syngenetic), so that the peat has previously been processed, appear to experience small losses.

Relative amount of C loss	Permafrost type	Landform Initiation	Number of years permafrost present	Number of years permafrost thawed (approx.)	General Location	Method
smaller	epigenetic (processed peat)	-450 – 550 CE (2400 – 1400 BP)	200-400	20 - 100	Fairbanks Alaska <sup>a</sup>	chronosequence
smaller	epigenetic (processed peat)	-6550 CE (8500 BP)	1800	30 – 200	AB, Canada <sup>b, c</sup>	chronosequence, <sup>14</sup> C
smaller	syngenetic and epigenetic (unprocessed and processed peat)	-5550 – -4650 CE (6600 – 7500 BP)	Unknown	20 - 130	NWT, Canada <sup>d</sup>	<sup>14</sup> C
larger	syngenetic (unprocessed peat)	-6050 – -8050 CE (8000 – 1000 BP)	8,000-10,000	30 - 1215	Koyukuk, Alaska <sup>e, f</sup>	chronosequence
larger	syngenetic (unprocessed peat)	-1050 – -50 CE (2000 – 3000 BP)	2,000-3,000	20 - 400	Innoko, Alaska <sup>f</sup>	chronosequence

<sup>a</sup>This study

<sup>b</sup>Heffernan et al. (2020)

<sup>c</sup>Estop-Aragonés et al. (2018)

<sup>d</sup>Estop-Aragones et al. (2018a), Wolfe et al. (2017)

<sup>e</sup>O'Donnell et al. (2012)

<sup>f</sup>Jones et al. (2017)

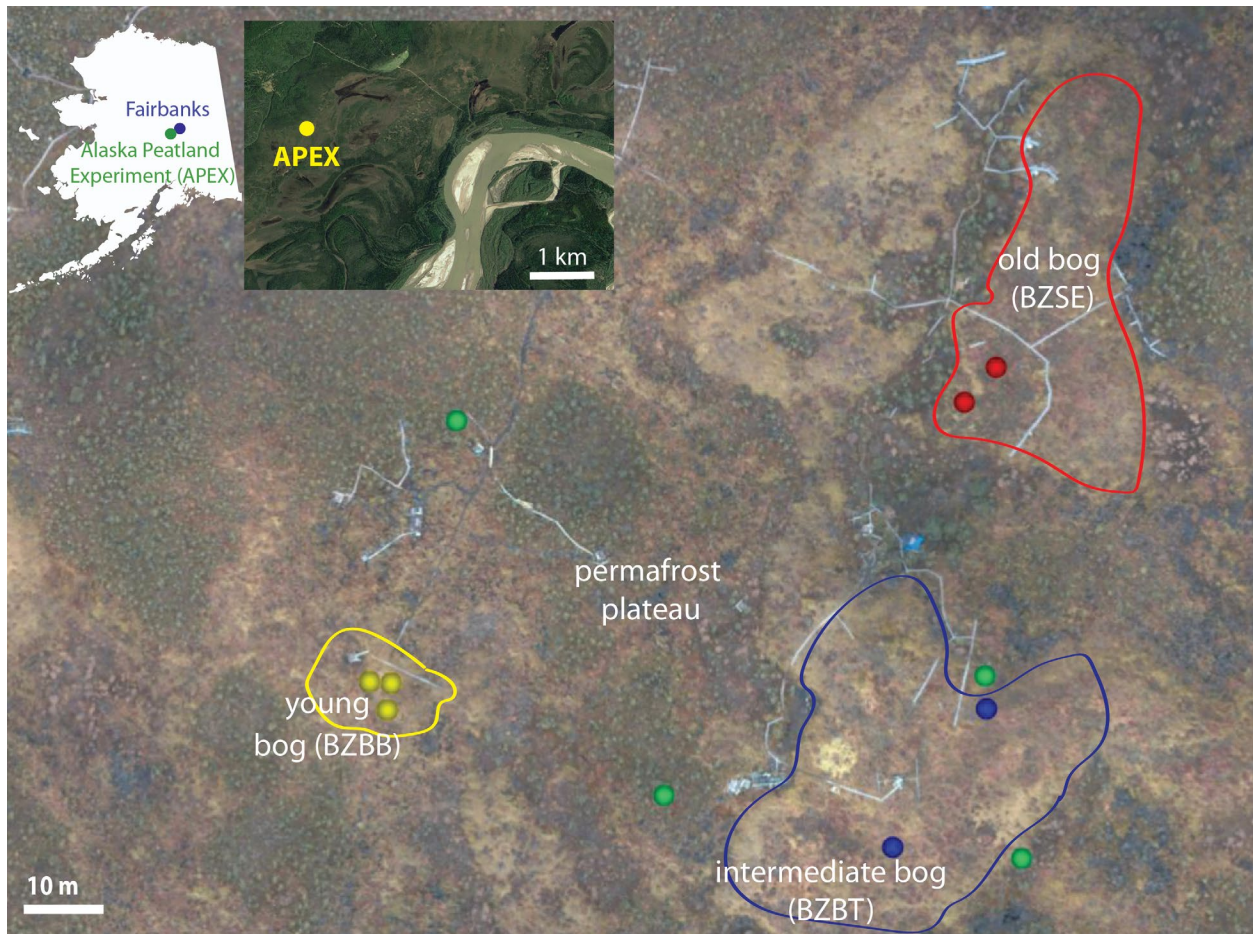


**Figure 1.** The Alaskan Peatland Experiment (APEX) site. This area is a mosaic of collapse-scar bogs within forested permafrost plateaus. Colors correspond to the different bogs: the 'old' bog is in red (BZSE), the 'intermediate' bog is in blue (BZBT), and the 'young' bog is in yellow (BZBB). Circles indicate the locations of the soil cores; green circles are cores taken from the permafrost plateau. Core numbers can be found in Figure S2. APEX is located near Fairbanks, close to the Tanana River, in the Interior of Alaska. Images: site - J. Hollingsworth; satellite - Google Earth.

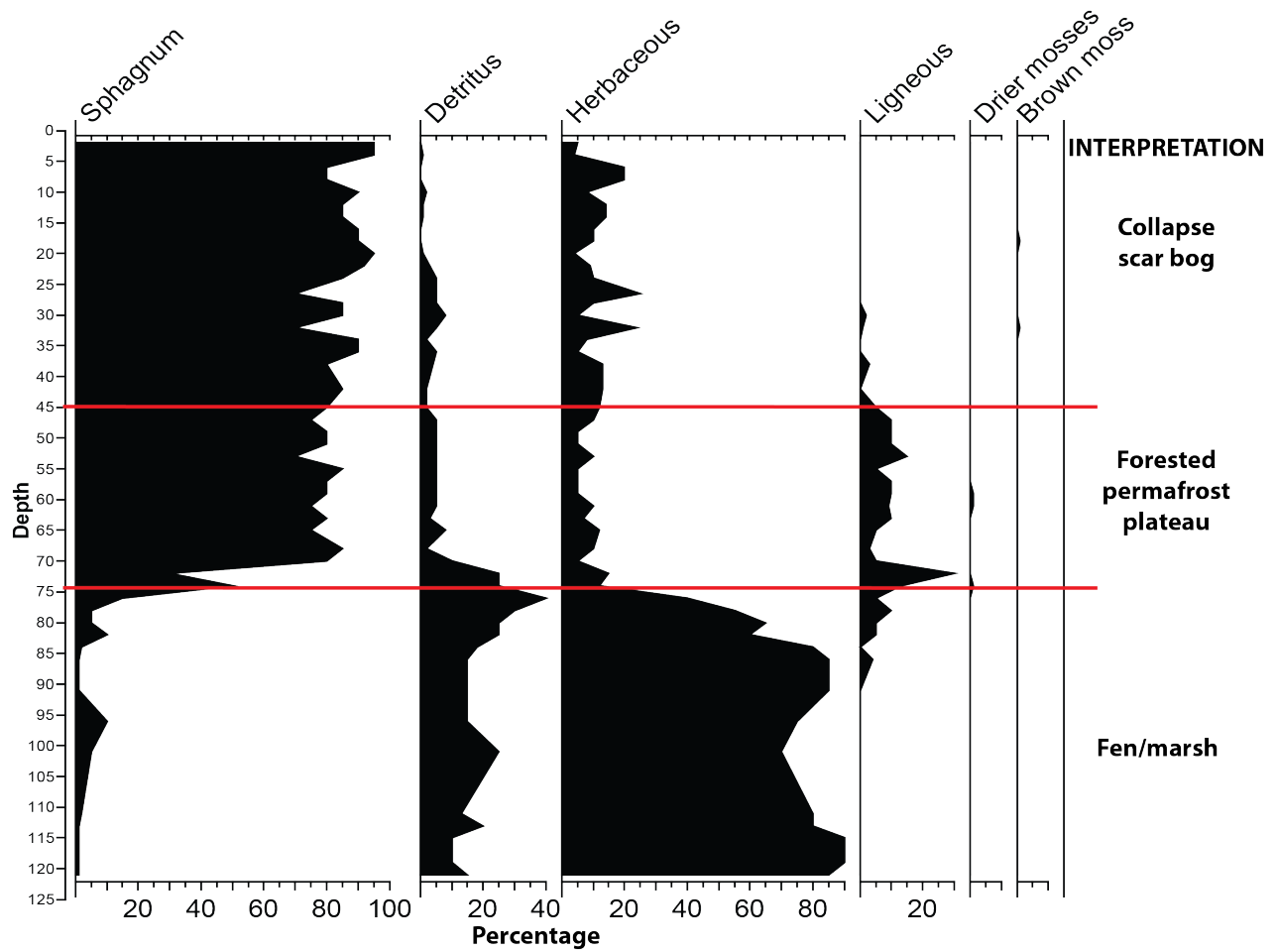


**Figure 2.** Simplified macrofossil diagram showing how changes in different amounts of material were used to determine the transitions between stratum ecosystems. Collapse scar bogs were dominated by bryophytic peat, while permafrost plateau forests had high levels of ligneous peat. At the base of all cores was material dominated by herbaceous peat from the initial fen/marsh period. This diagram is for the Young bog-4 core (BB4). Full macrofossil diagrams can be found in Figure S7.

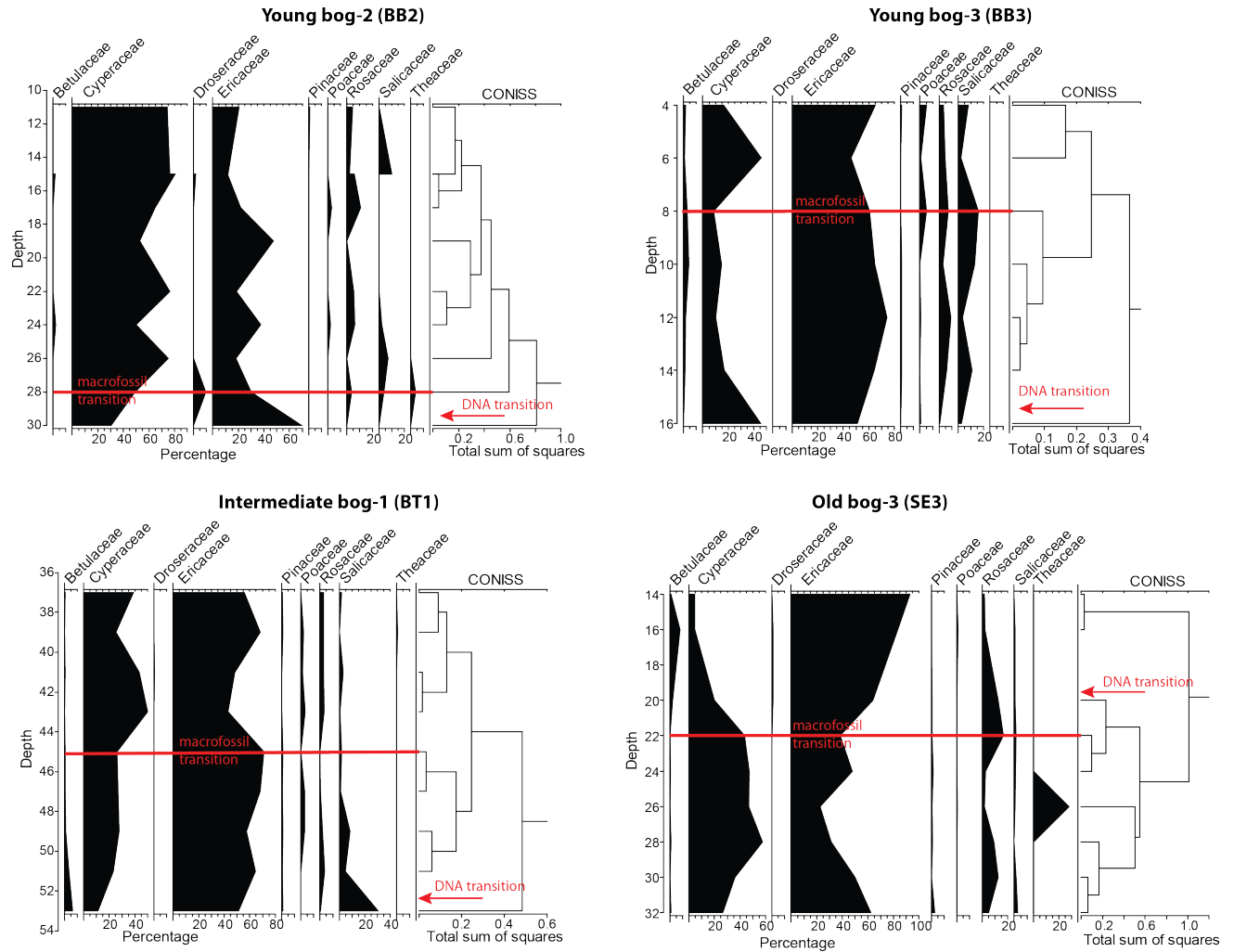


**Figure 3.** Vegetation transition analysis from peat cores using CONISS analysis of plant DNA at the family level. The red lines indicate the depths of macrofossil-based strata transitions, while the red arrows indicate where the CONISS analyses indicates the first break in the DNA data.

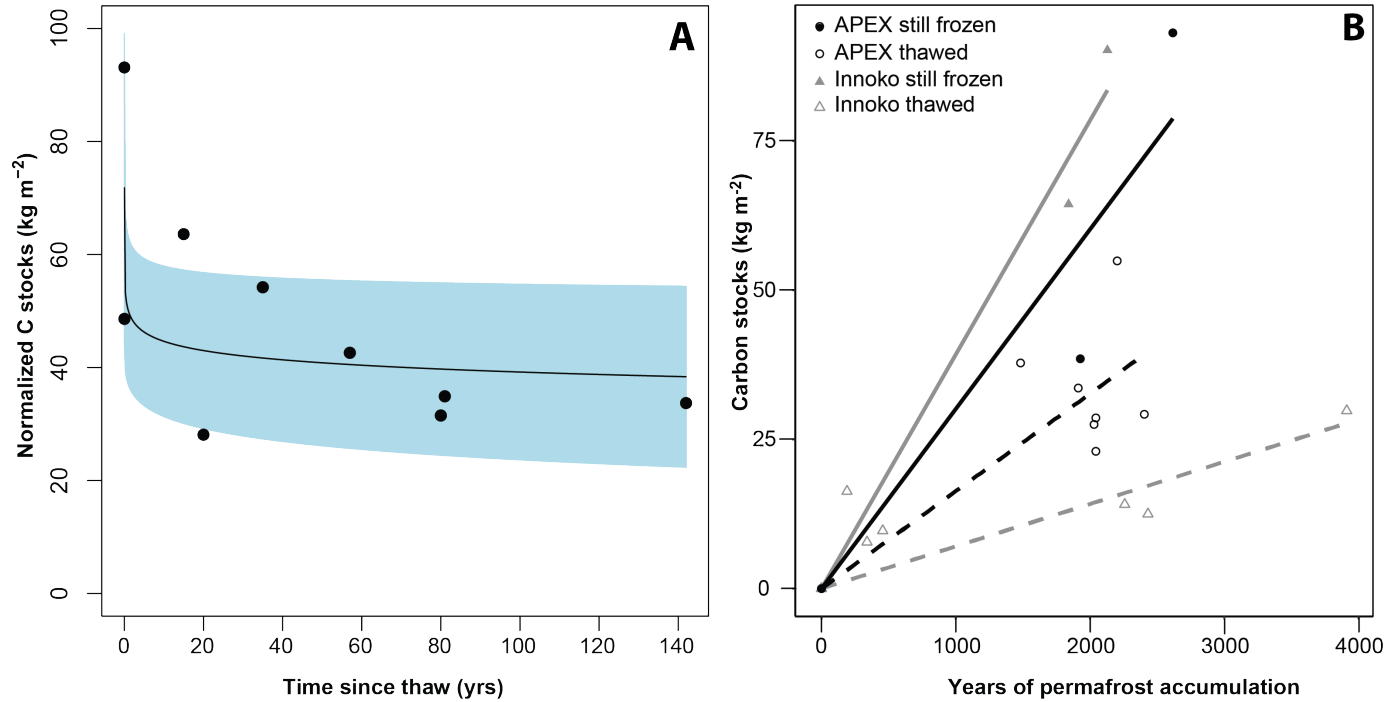


**Figure 4.** Estimating carbon losses from APEX permafrost using two methods. A) The Normalized C method, where C stocks were normalized to the oldest core and then plotted against the number of years each core has been thawed (see methods). This method shows a 34% loss of C with time. B) The linear method comparing stocks between still frozen peat (solid lines) and thawed peat (dashed lines) for both the APEX site (black, this study) and Innoko, AK (gray, Jones et al., 2017). With C loss, the slope of the line representing thawed cores (dashed line) will have a lower slope than the slope of the line where the cores still contain permafrost (solid line). Using this method APEX C losses are estimated at 46% of the existing stocks, but lower than losses of C found for Innoko.

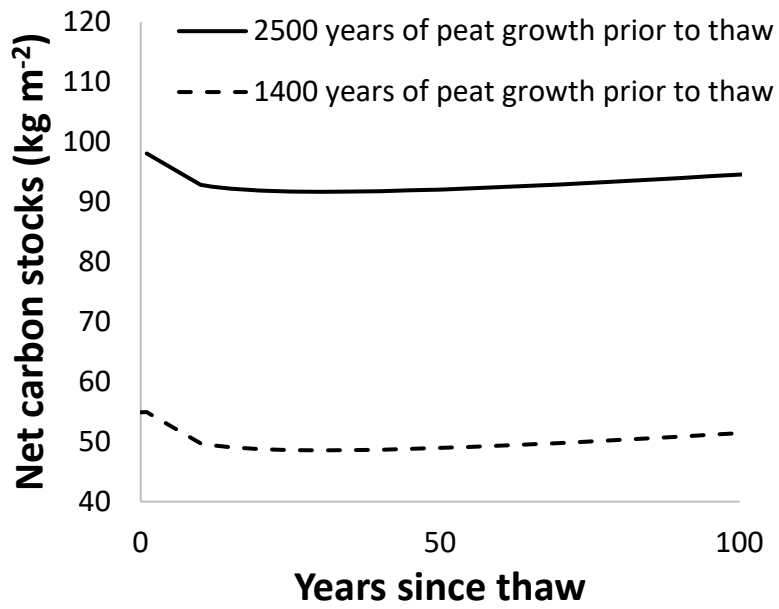


**Figure 5.** Net C stocks, modeled as inputs from bog C and losses due to permafrost thaw for two time periods, which represent the upper and lower estimates of that at which peat initiated.

## SUPPLEMENTAL INFORMATION

### 1 <sup>210</sup>Pb and <sup>7</sup>Be analysis

2 <sup>7</sup>Be, which has similar atmospheric depositional source as <sup>210</sup>Pb but a much shorter half-life (53 days vs  
 3 22.1 years), was used constrain if there was downward movement of fallout radionuclide bearing  
 4 particles through our soil profiles over the mean life of <sup>7</sup>Be. Four additional surface cores (for measuring  
 5 <sup>7</sup>Be activity) were taken at the Intermediate bog location (BZBT) over a period of ~5 months the summer  
 6 of 2015 by cutting blocks of peat out of the bog. Each core was divided into horizons, most between 2-5  
 7 cm thick, and analyzed for bulk density. We found <sup>7</sup>Be down to 7 cm (Figure S1). This depth is similar to,  
 8 but on the shallow end, for values found within bogs and fens in Sweden (8 - 20 cm; Hansson et al.,  
 9 2014). Based on our measurements in early May, there does not appear to be large inputs of <sup>7</sup>Be in late  
 10 season snowfall (Figure S1). Early summer rain events were the main source of <sup>7</sup>Be (and thus <sup>210</sup>Pb) into  
 11 the soil, transporting <sup>7</sup>Be up to 7 cm into the soil. We see penetration of <sup>7</sup>Be in August or September  
 12 only to 4 cm due to the many small rain events during this time, which resulted in lower deposition of  
 13 <sup>7</sup>Be and likely less downward transport into the soil. Because <sup>7</sup>Be is a short-lived radionuclide, these data  
 14 do not provide information about the inputs from earlier in the winter. Attempts to model this  
 15 downwash affect for <sup>210</sup>Pb using two different ages models was not successful (Manies et al, 2016).  
 16 Therefore, we did not include <sup>210</sup>Pb data in our age modeling for our soil cores, instead relying solely on  
 17 <sup>14</sup>C data.

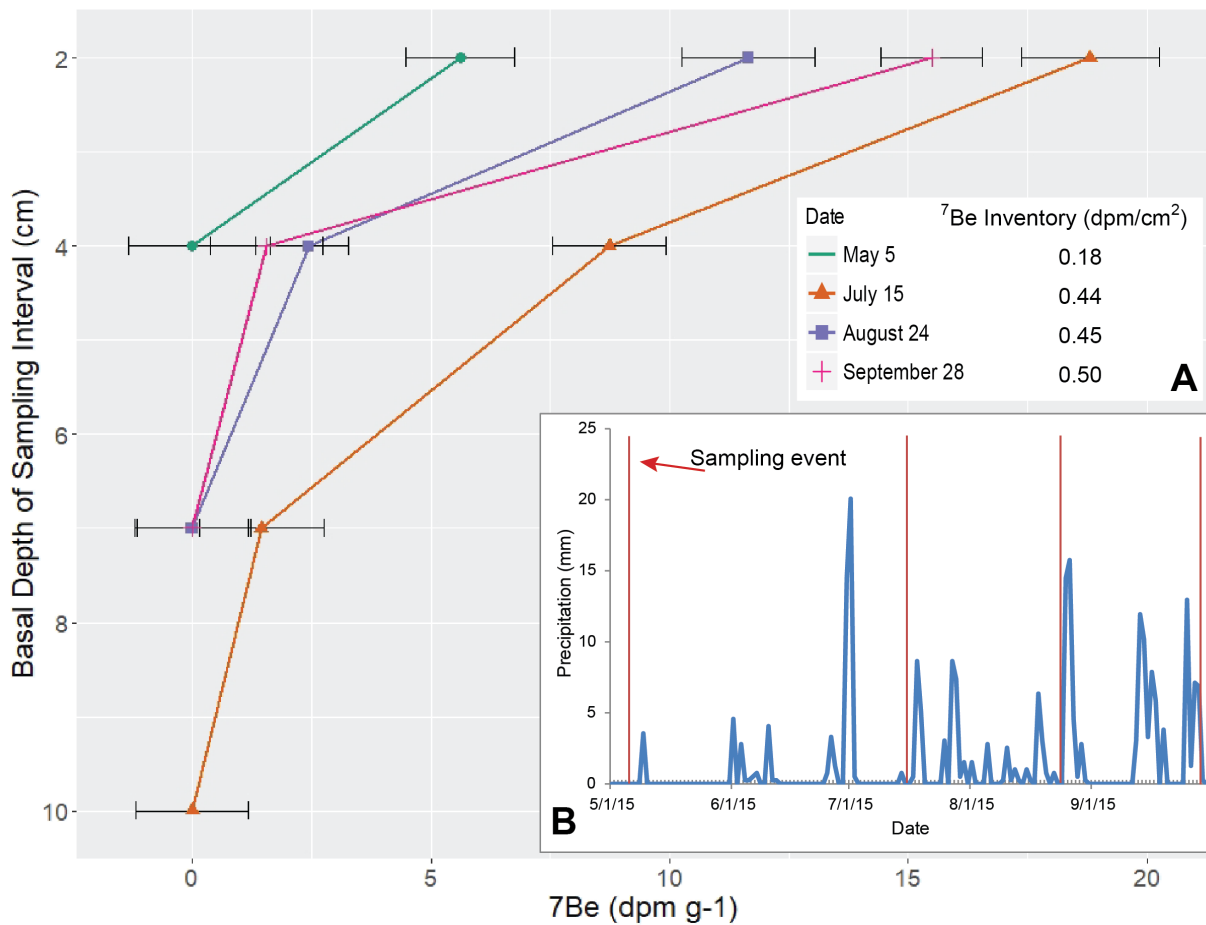
18  
 19 **Table S1.** A comparison of age estimates using <sup>14</sup>C data (either from Calibomb or Calib; see Table S2) and  
 20 date estimates for base depth of selected core intervals from the CRS model using <sup>210</sup>Pb data. The  
 21 tendency of the <sup>210</sup>Pb ages to be younger than <sup>14</sup>C ages, in addition to finding <sup>210</sup>Pb deep within our soil  
 22 cores, led us to suspect that <sup>210</sup>Pb was mobile in these sites. This hypothesis was confirmed using <sup>7</sup>Be  
 23 (see above text).

Core ID	Depth Range (cm)	Fraction Modern	<sup>14</sup> C date range (yr)	<sup>210</sup> Pb date	<sup>210</sup> Pb error (yrs)	<sup>210</sup> Pb older or younger than <sup>14</sup> C age?
BZBB 2	24-26	1.1040	1996.1– 2000.1	1999.2	1.3	same
BZBB 4	26-28	1.1080	1995.6 – 1999.3	1994.6	2.7	older
	36-38	1.211	1983.9 – 1986.2	1982.5	4.5	older
	72-74	1.0054	1954.9 – 1956.4	1944.1	20.5	older
BZBT 1	32-34	1.2410	1982.0 – 1984.1	1988.8	1.3	younger
	40-45	1.0535	1956.6 – 1957.2	1981.8	3.3	younger
	50-55	0.9864	1802 – 1938	1940.6	33.6	younger
	65-70	0.9521	1439 – 1522	1915.5	42.4	younger
BZBT 9	35-40	1.5671	1968.1 – 1970.1	2001.1	0.5	younger
	47-49	0.9796	1725 - 1787	1999.8	0.6	younger
	80-85	0.9852	1726 - 1814	1974.1	2.3	younger
BZBT 11	31-32	0.9749	1736 - 1805	1912.2	30.0	younger
BZSE 4	42-44	1.003	1954.8 – 1956.0	1942.8	14.0	older
	54-56	0.9758	1619 - 1670	1901.3	108.0	younger

24  
 25

**SUPPLEMENTAL INFORMATION**

26 **Figure S1.**  $^7\text{Be}$  with depth for four timepoints within the summer of 2015 at the BZBT 1 site. The deeper  
 27 movement of  $^7\text{Be}$  within the soil profile may be correlated with the precipitation (A), with sampling  
 28 events noted by the red lines. The integrated  $^7\text{Be}$  inventory (B) shows increase over time reflecting  
 29 ongoing input from atmospheric deposition that exceeds decay of previously deposited  $^7\text{Be}$  activity.



## SUPPLEMENTAL INFORMATION

**Table S2.** Radiocarbon laboratory data. Dates were obtained from three labs: 1) LLNL: samples were prepared and analyzed at the Center for Accelerator Mass Spectrometry (CAMS) at the Lawrence Livermore National Laboratory (LLNL), 2) USGS: sample preparation occurred at the U.S. Geological Survey Radiocarbon Laboratory, while samples were analyzed at the CAMS LLNL, and 3) Beta: samples were prepared and analyzed at Beta Analytic (Miami, FL). Fraction Modern values and errors not given in the data report were calculated using CALIBomb (<http://calib.org/CALIBomb/>) using intercal13 as the pre-bomb calibration data set and NZ1 as the post-bomb calibration data set. Samples labeled BZBB are from the young bog, BZBT 1 & BZBT 9 are from the intermediate bog, and BZSE are from the old bog. Samples from BZBT 11 and BZGT are from the forest permafrost plateau.

Sample Name	Depth Range (cm)	Description	Lab #	14C age	14C age error	Fraction Modern	Modern error
BZBB 2.26	24-26	<i>Sphagnum riparium</i>	LLNL-177606	>modern	-	1.1040	0.0032
BZBB 2.40	39-42	<i>Vaccinium oxycoccus</i> leaves, <i>Picea mariana</i> needles	Beta-397861	-	-	1.2392	0.0046
BZBB 2.106	103-106	charcoal	LLNL-177605	2125	25	0.7675	0.0022
BZBB 3.14	12-14	<i>Picea mariana</i> branchlet	LLNL-177608	>modern	-	1.1815	0.0038
BZBB 3.53	50-53	charcoal	LLNL-177609	115	25	0.9858	0.0028
BZBB 3.80	77-80	charcoal	LLNL-177610	1615	25	0.8179	0.0023
BZBB 3.116+	116 - ~117	charcoal	LLNL-177607	4230	25	0.5906	0.0017
BZBB 4b.28 Suppl	26-28	<i>Picea mariana</i> needles, unidentified leaf fragment, <i>Sphagnum</i> spp. leaves & stems	Beta-399724	-	-	1.1175	0.0028
BZBB 4b.32	30-32	<i>Picea mariana</i> needle, leaf fragment, <i>Sphagnum</i> spp. stems	Beta-397863	-	-	1.1217	0.0045
BZBB 4b.38	36-38	<i>V. oxycoccus</i> leaves, <i>Picea mariana</i> needles, <i>Sphagnum</i> spp. stems	Beta-397864	-	-	1.2207	0.0030
BZBB 4.74	72-74	<i>Sphagnum</i> spp. stems, shrub leaves	LLNL-177611	modern	-	1.0054	0.0029
BZBB 4.78	76-78	<i>Sphagnum</i> spp. stems, charcoal	Beta-415694	200	30	0.98302	0.0036
BZBB 4.121	119-121	charcoal	LLNL-179988	2425	30	0.7395	0.0026
BZBB 4.136	128-136	charcoal	Beta-415693	3540	30	0.6486	0.0024
BZBT 1.33	32-34	Undifferentiated plant material	USGS-9502	>modern	-	1.2410	0.0035
BZBT 1a.45	40-45	<i>Sphagnum</i> spp. stems	LLNL-177615	>modern	-	1.0535	0.0030
BZBT 1a.55	50-55	<i>Vaccinium</i> spp. leaves	LLNL-177034	110	30	0.9864	0.0035

**SUPPLEMENTAL INFORMATION**

BZBT 1a.70	65-70	plant material	USGS-9503	395	30	0.9521	0.0031
BZBT 1.117	117-119	charcoal	LLNL-179989	1975	30	0.7819	0.0027
BZBT 1a.122	117-122	charcoal	USGS-9504	2005	25	0.7793	0.0024
BZBT 9a.40	35-40	plant material	USGS-9506	>modern	-	1.5672	0.0045
BZBT 9.49	47-49	<i>Picea mariana</i> needles	USGS-9263	165	25	0.9796	0.0027
BZBT 9a.85	80-85	charcoal	Beta-417890	180	30	0.9852	0.0037
BZBT 9a.100	95-100	charred wood	USGS-9507	240	25	0.9705	0.0028
BZBT 9b.130	124-130	charred wood	USGS-9505	1885	25	0.7909	0.0023
BZBT 11.32	31-32	Unidentified plant material	USGS-9813	205	25	0.9749	0.0029
BZBT 11.56	55-56	charcoal	Beta-417888	1440	30	0.8421	0.0031
BZBT 11.116+	116- ~117	charcoal	Beta-417889	4020	30	0.6108	0.0023
BZSE 3.26	24-26	<i>Picea mariana</i> needles, <i>Vaccinium</i> spp. leaves	Beta-397860	-	-	1.1848	0.0029
BZSE 3.36	34-36	moss, leaves	LLNL-177618	>modern	-	1.7451	0.0050
BZSE 3.70	65-70	charcoal, Undifferentiated shrub leaf fragments, <i>Carex</i> spp. seed	LLNL-177619	560	25	0.9328	0.0028
BZSE 3.140+	140- ~141	charcoal	LLNL-177617	2895	25	0.6976	0.0020
BZSE 4c.44	42-44	<i>Sphagnum</i> spp. stems, <i>Picea</i> needles	Beta-415691	-	-	1.0116	0.0025
BZSE 4.56 Suppl	54-56	<i>V. oxycoccus</i> leaves, <i>Picea mariana</i> needles, undifferentiated leaf fragments, <i>Aulacomnium palustre</i> leaves & stems	Beta-399723	260	30	0.9758	0.0036
BZSE 4.69	67-69	<i>Picea mariana</i> needle, undifferentiated leaf fragment	Beta-397857	170	30	0.9868	0.0037
BZSE 4.73 Suppl	71-73	<i>Betula</i> spp. seeds, <i>Picea</i> spp. needle fragments, <i>Aulacomnium palustre</i> stems & leaves, undifferentiated shrub leaf fragments	Beta-399725	80	30	0.9979	0.0037
BZSE 4.86	84-86	charred leaf and wood fragments	Beta-397859	480	30	0.9494	0.0035
BZSE 4.93	90-93	charcoal	LLNL-177621	310	25	0.9620	0.0028
BZSE 4.130	127-130	<i>Picea</i> spp. needles, undifferentiated shrub leaves	LLNL-177620	490	35	0.9407	0.0036

**SUPPLEMENTAL INFORMATION**

BZSE 4.146	144-146	<i>Sphagnum</i> spp. stems, charcoal	Beta-415392	2130	30	0.7732	0.0029
BZGC 11.24	22-24	<i>Sphagnum</i> spp. stems	LLNL-176602	>modern	-	1.6362	0.0057
BZGC 11.48	48-50	<i>Sphagnum</i> spp. stems	LLNL-176603	1500	30	0.8295	0.0028
BZGC 11.55	54-55	<i>Sphagnum</i> spp. stems	LLNL-177024	1130	40	0.8689	0.0042
BZGC 11.65	64-66	<i>Sphagnum</i> spp. stems	LLNL-176604	4290	70	0.5863	0.0044
BZGC 11.76	77-78	charcoal	LLNL-177025	1870	30	0.7926	0.0028
BZGC 11.94	94-95	bulk peat	LLNL-179990	2475	30	0.7347	0.0025
BZGC 11.96	97-98	charcoal	LLNL-176605	4385	30	0.5782	0.0022

## SUPPLEMENTAL INFORMATION

**Figure S2.** Map of landform age (cal BP) based on Bacon model output with the *wmean* values presented first and the maximum and minimum age estimates within parentheses. Green circles indicate areas that still contain permafrost. The other colors represent cores taken from different bogs. Circles without values were not age dated.



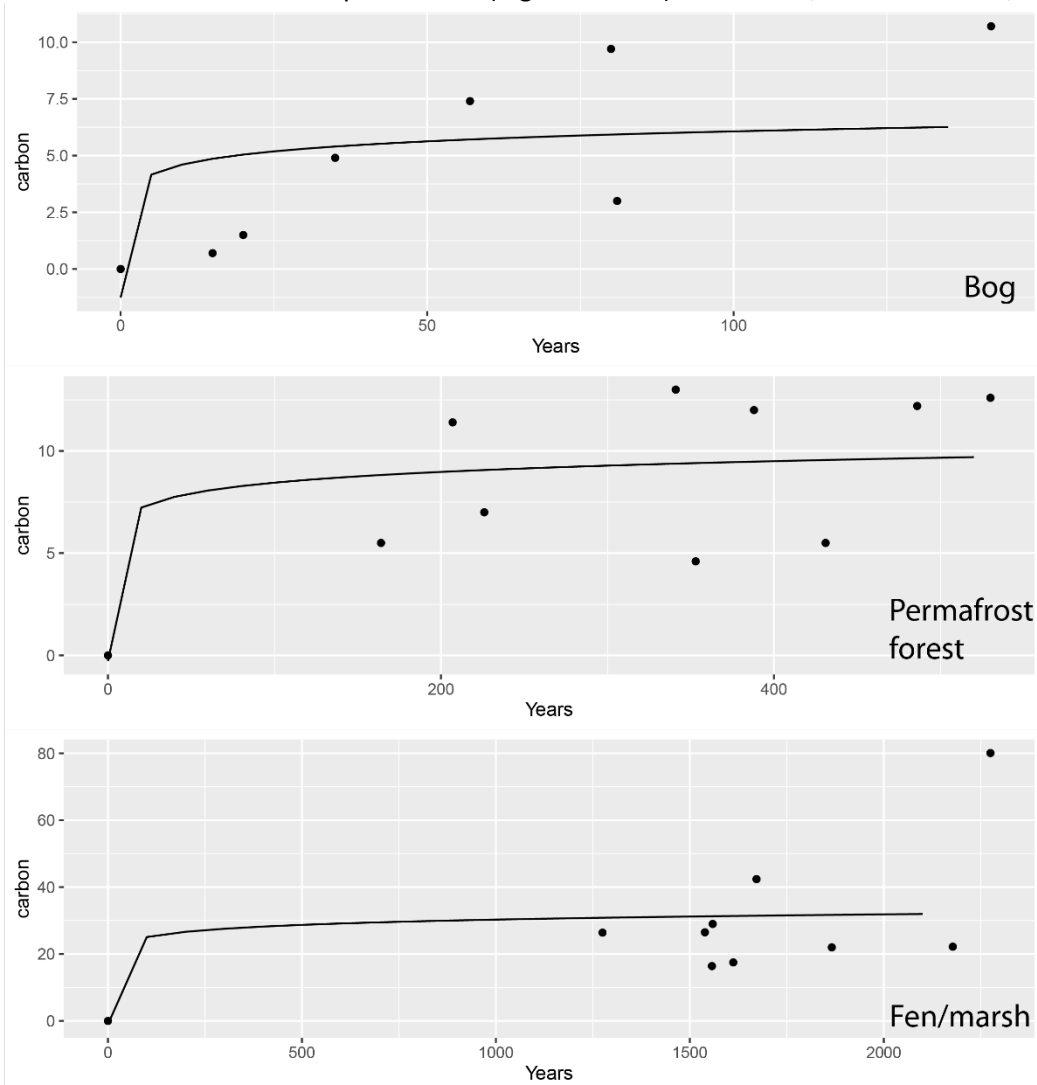
## SUPPLEMENTAL INFORMATION

**Figure S3.** Map of permafrost thaw based on bacon model output with the *wmean* values presented first and the maximum and minimum age estimates within parentheses. Colors represent cores taken from different locations. The green circles do not have values as these sites still contain permafrost.



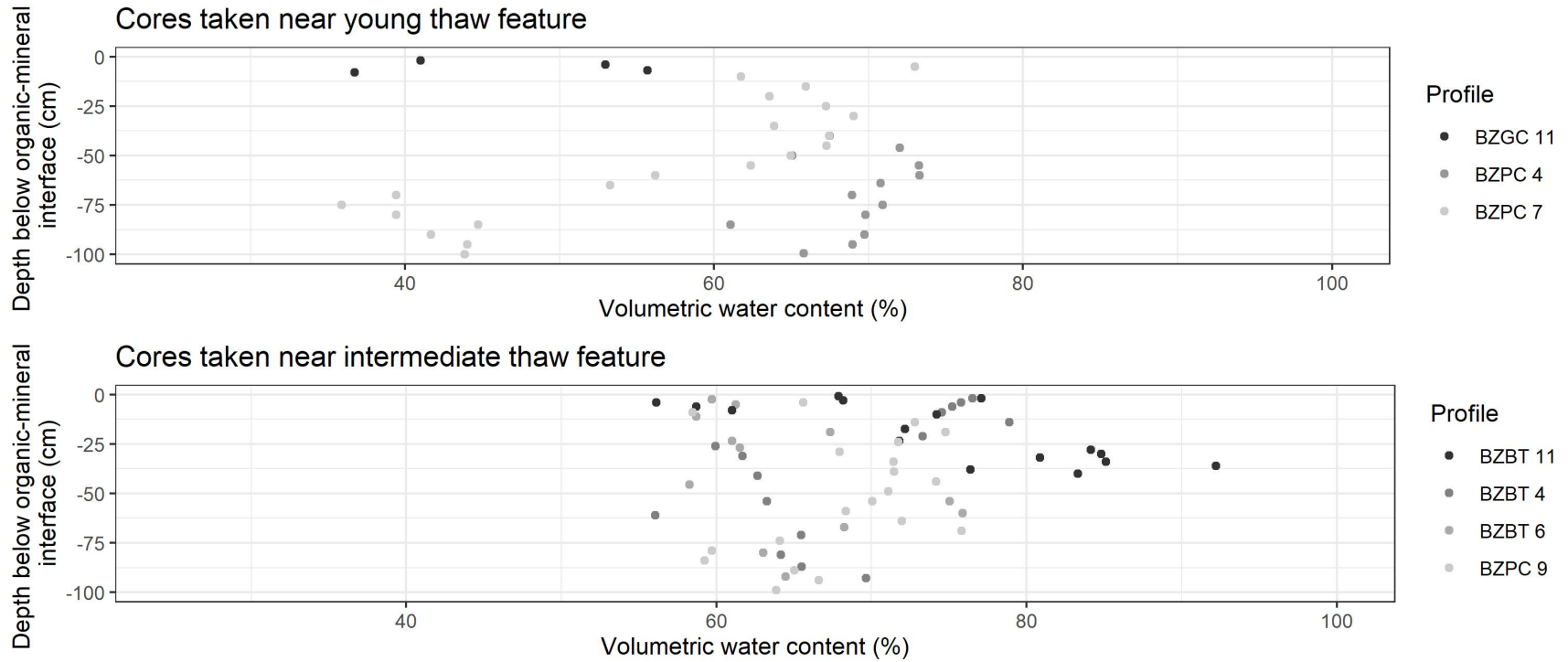
## SUPPLEMENTAL INFORMATION

**Figure S4.** Carbon stocks over time by stratum with logarithmic fits. Bog parameters (polynomial fit): Intercept = -0.1551,  $x = 0.1196$ ,  $x^2 = -0.0003$ . Permafrost forest parameters (logarithmic fit):  $a = 0.7575$ ,  $b = 4.9613$ . Fen/marsh parameters (logarithmic fit):  $a = 2.266$ ,  $b = 14.646$ .



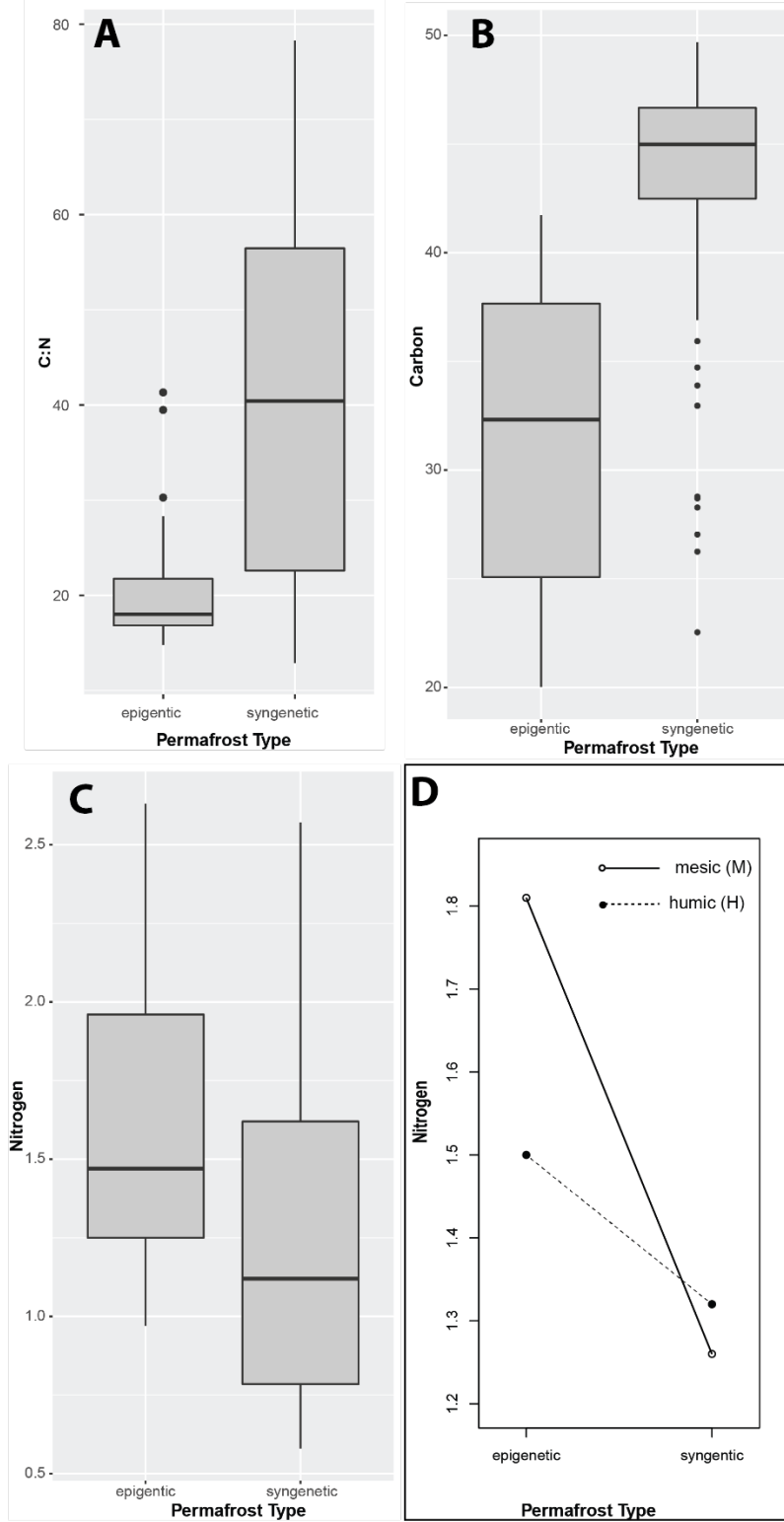
## SUPPLEMENTAL INFORMATION

**Figure S5.** Plot of volumetric water content, which is correlated to ice content, for the mineral soil from cores taken in two places: (top) close to the young thaw feature, which had slow expansion, and (bottom) close to the intermediate thaw feature, which experienced much quicker expansion.



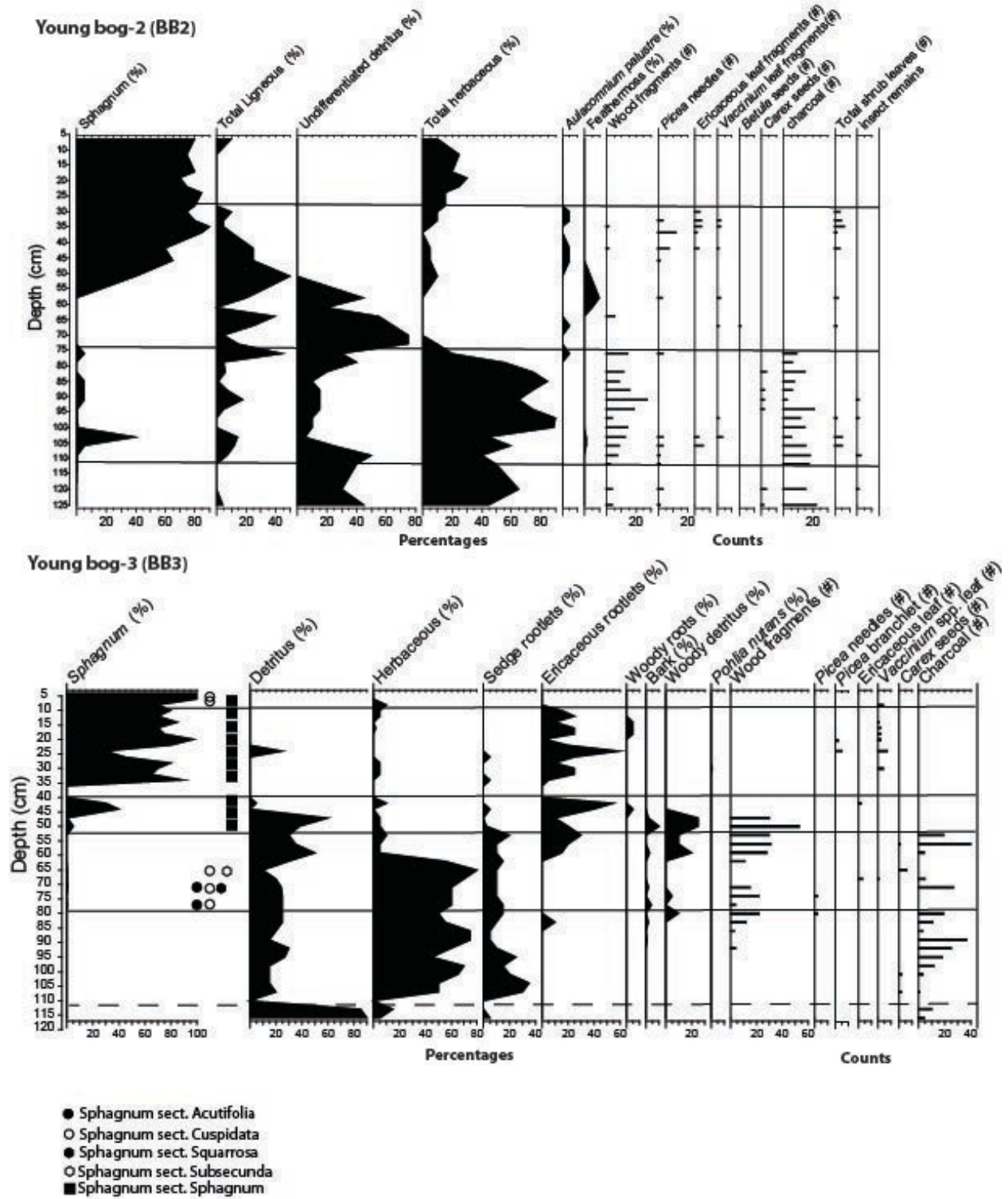
## SUPPLEMENTAL INFORMATION

**Figure S6.** Comparison of organic soil between epigenetic permafrost (this study, APEX) and syngenetic permafrost (Innoko and Koyukuk, AK; Jones et al, 2016) for (A) C:N ratios, (B) C concentrations, and (C) N concentrations. We also found a permafrost type by horizon (Manies, 2020) interaction for Nitrogen.



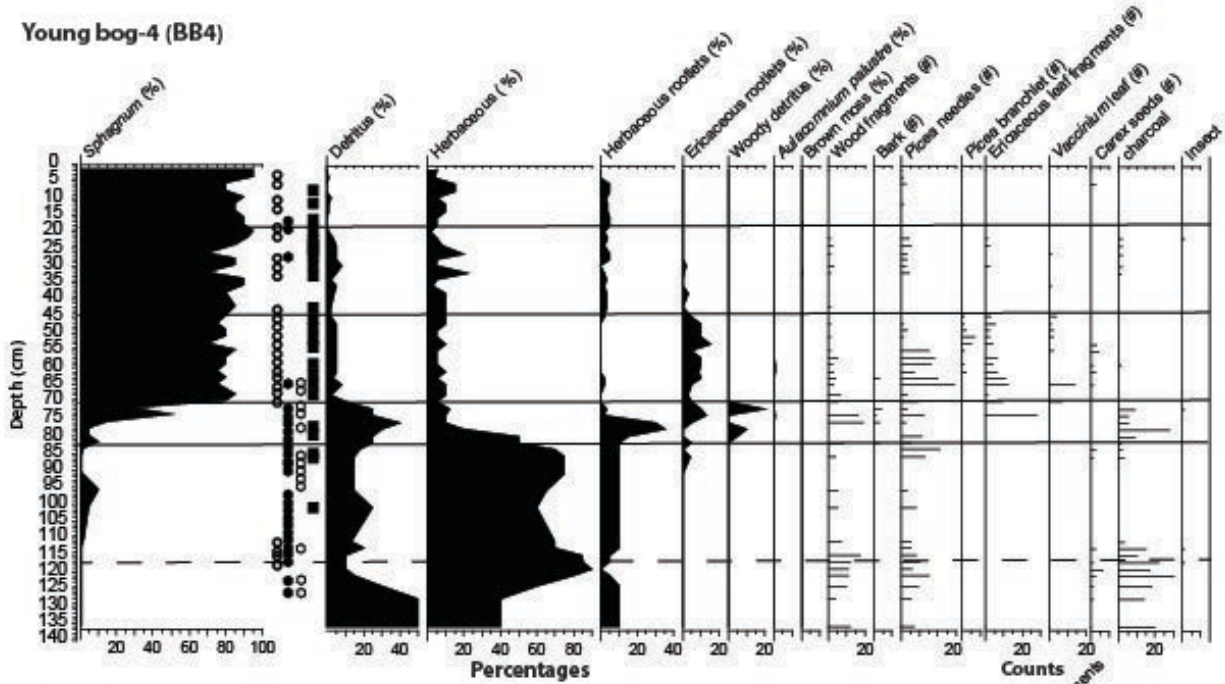
SUPPLEMENTAL INFORMATION

Figure S7. Macrofossil diagram of cores showing percentage and count data for material found within each sample.

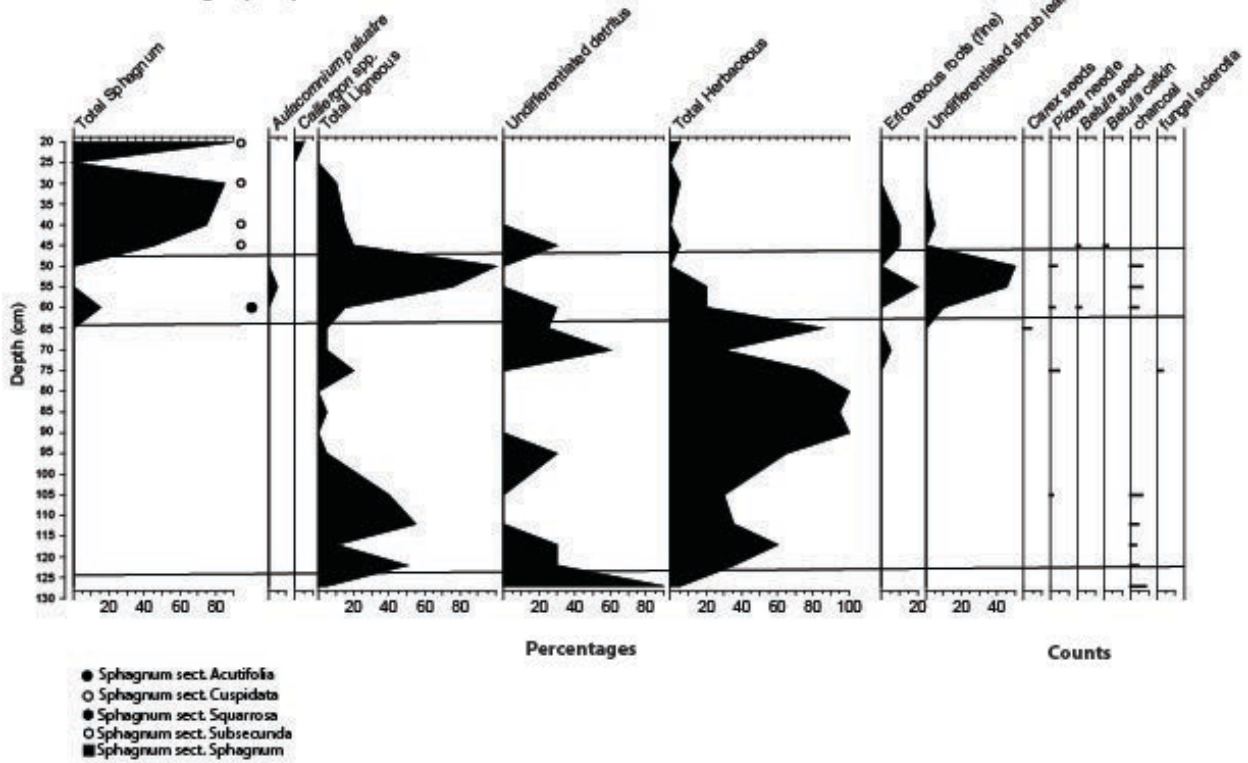


# SUPPLEMENTAL INFORMATION

Young bog-4 (BB4)

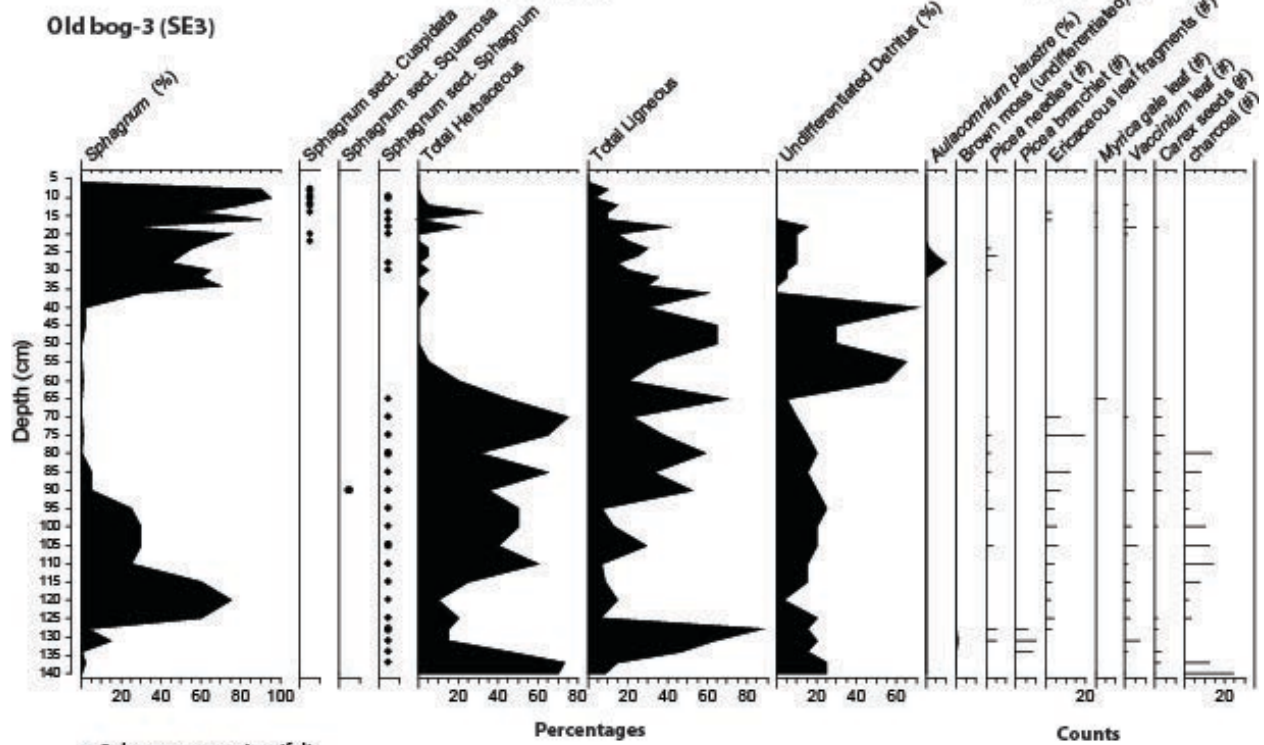
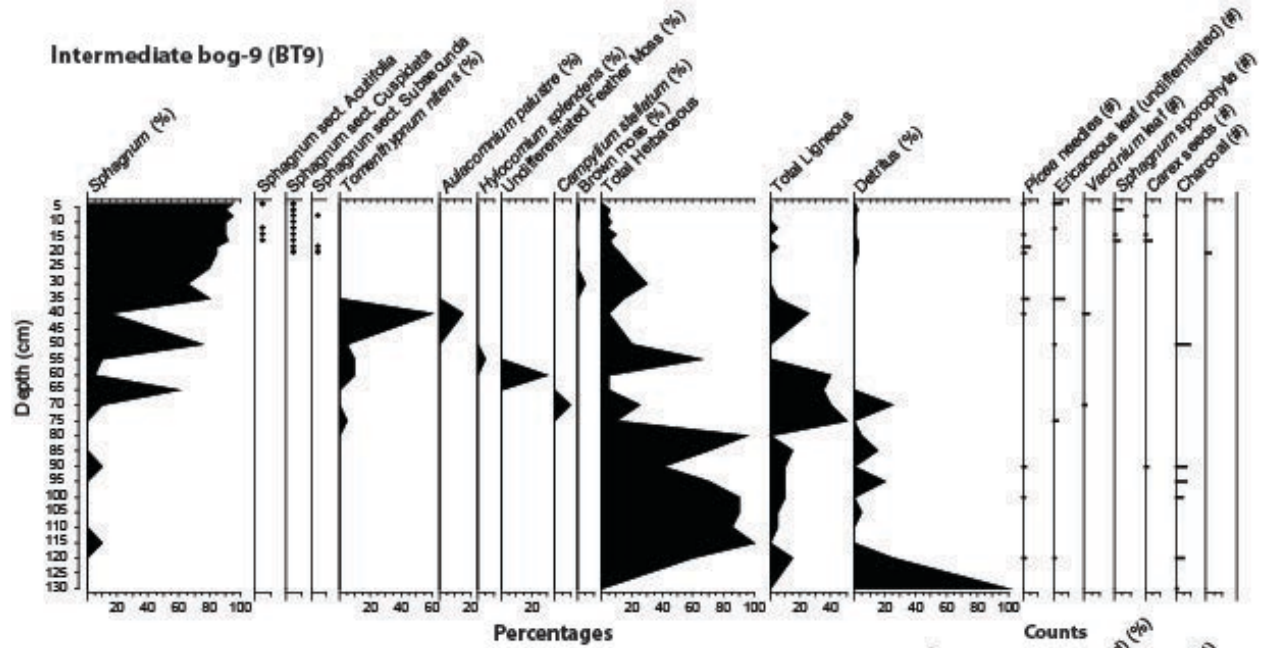


Intermediate bog-1 (BT1)



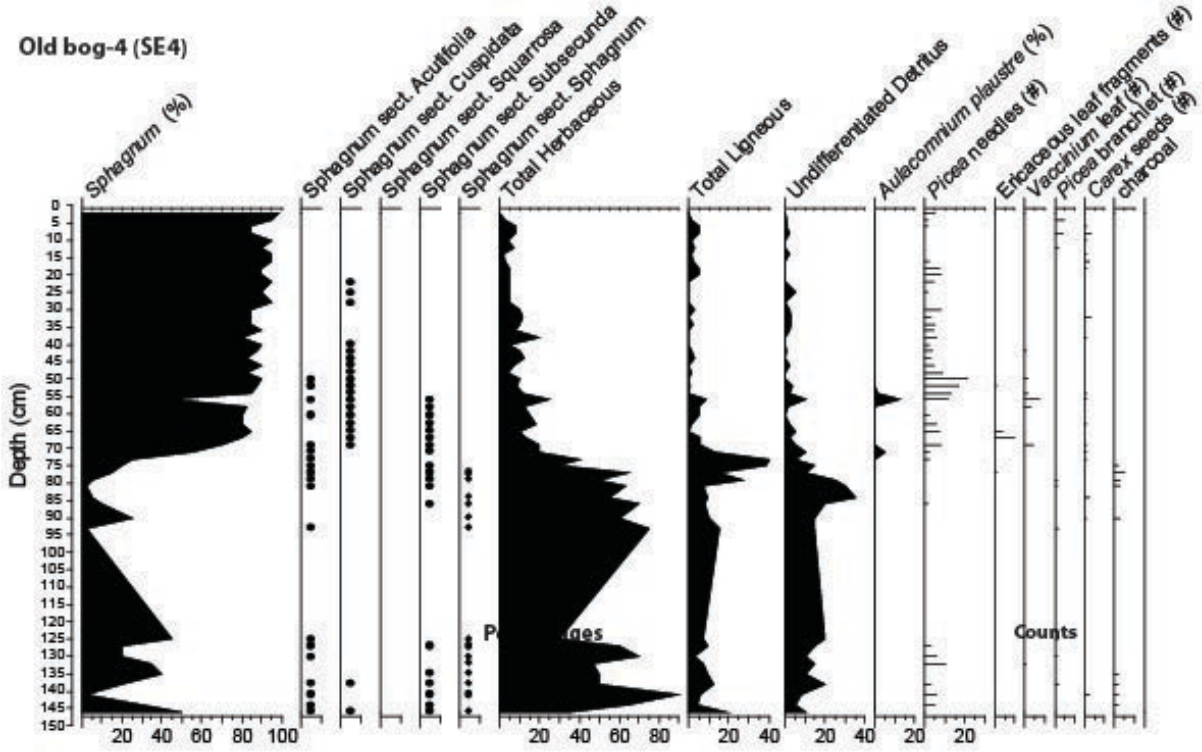
- Sphagnum sect. Acutifolia
- Sphagnum sect. Cuspidata
- Sphagnum sect. Squarrosa
- Sphagnum sect. Subsecunda
- Sphagnum sect. Sphagnum

SUPPLEMENTAL INFORMATION



- Sphagnum sect. Acutifolia
- Sphagnum sect. Cuspidata
- Sphagnum sect. Squarrosa
- Sphagnum sect. Subsecunda
- Sphagnum sect. Sphagnum

SUPPLEMENTAL INFORMATION



Permafrost plateau (BT-11)

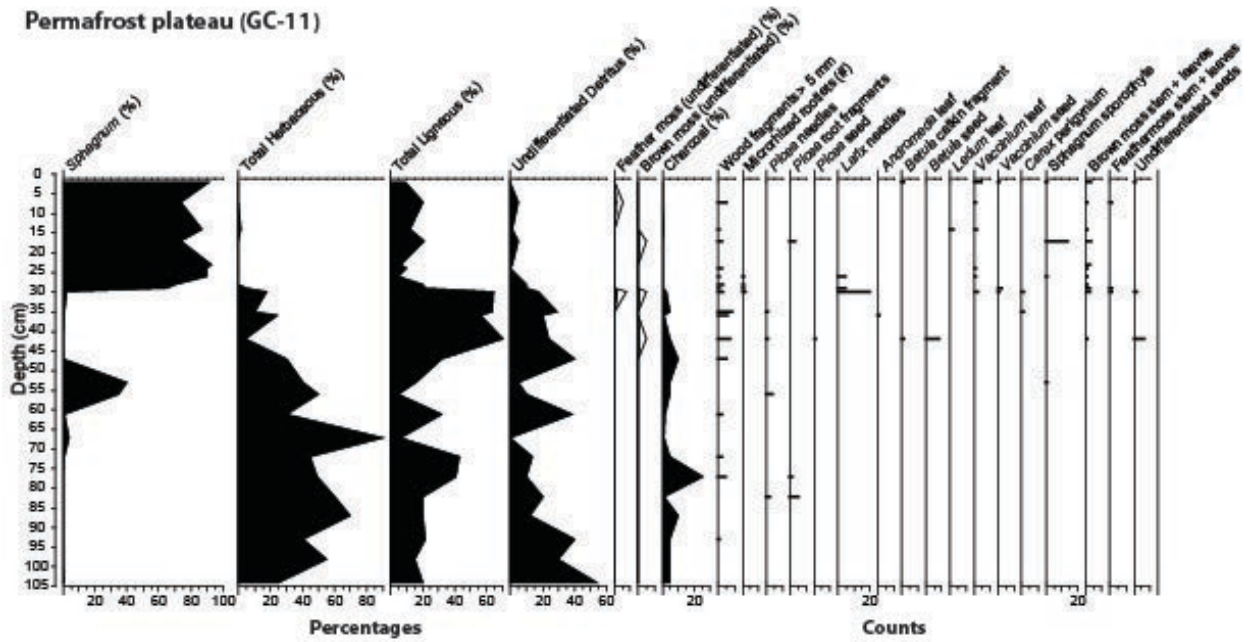
- Sphagnum sect. Acutifolia
- Sphagnum sect. Cuspidata
- Sphagnum sect. Squarrosa
- Sphagnum sect. Subsecunda
- Sphagnum sect. Sphagnum

Percentages

Counts

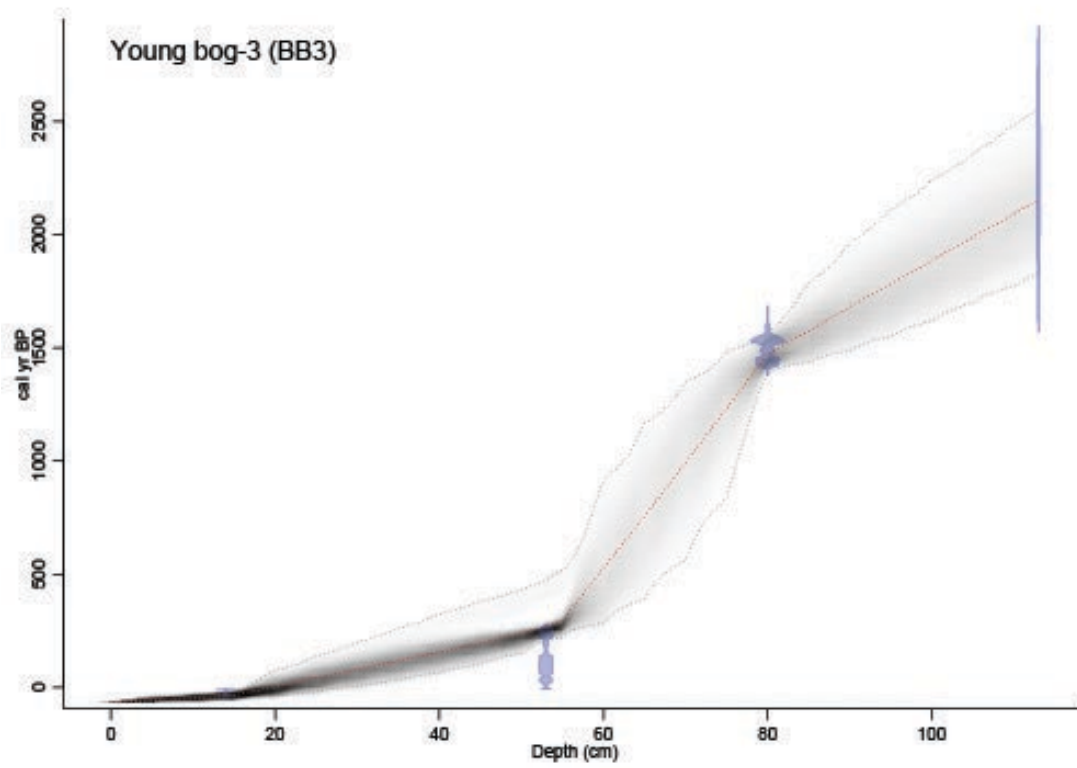
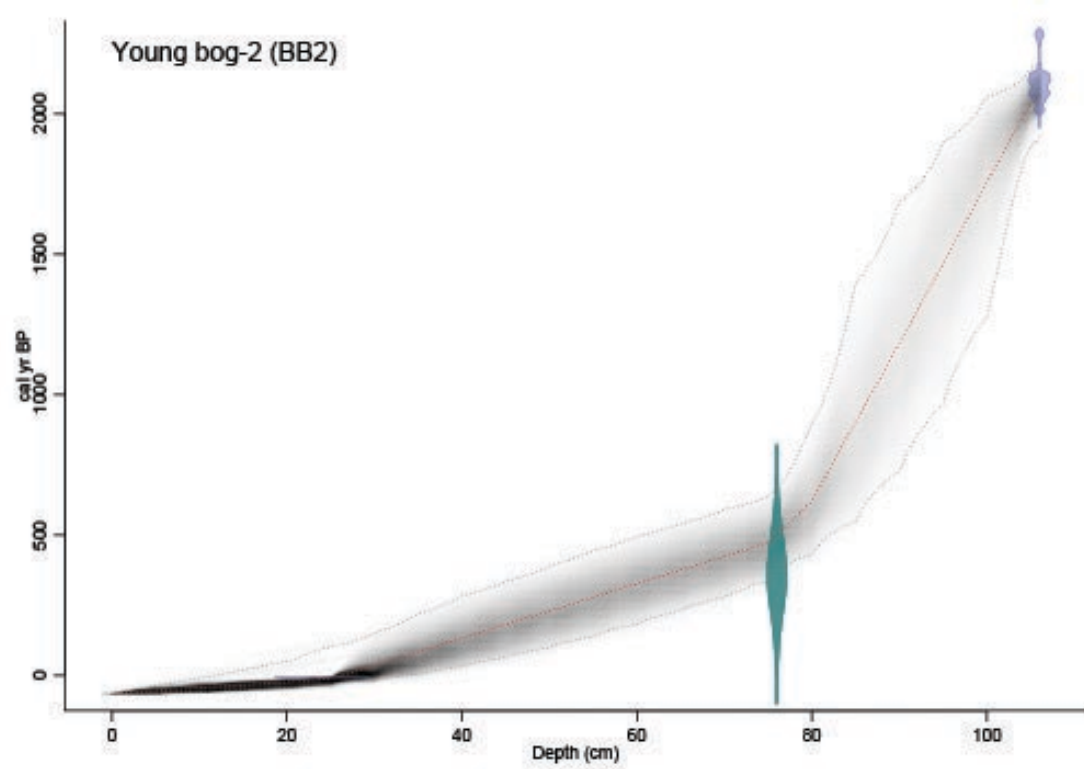
# SUPPLEMENTAL INFORMATION

## Permafrost plateau (GC-11)

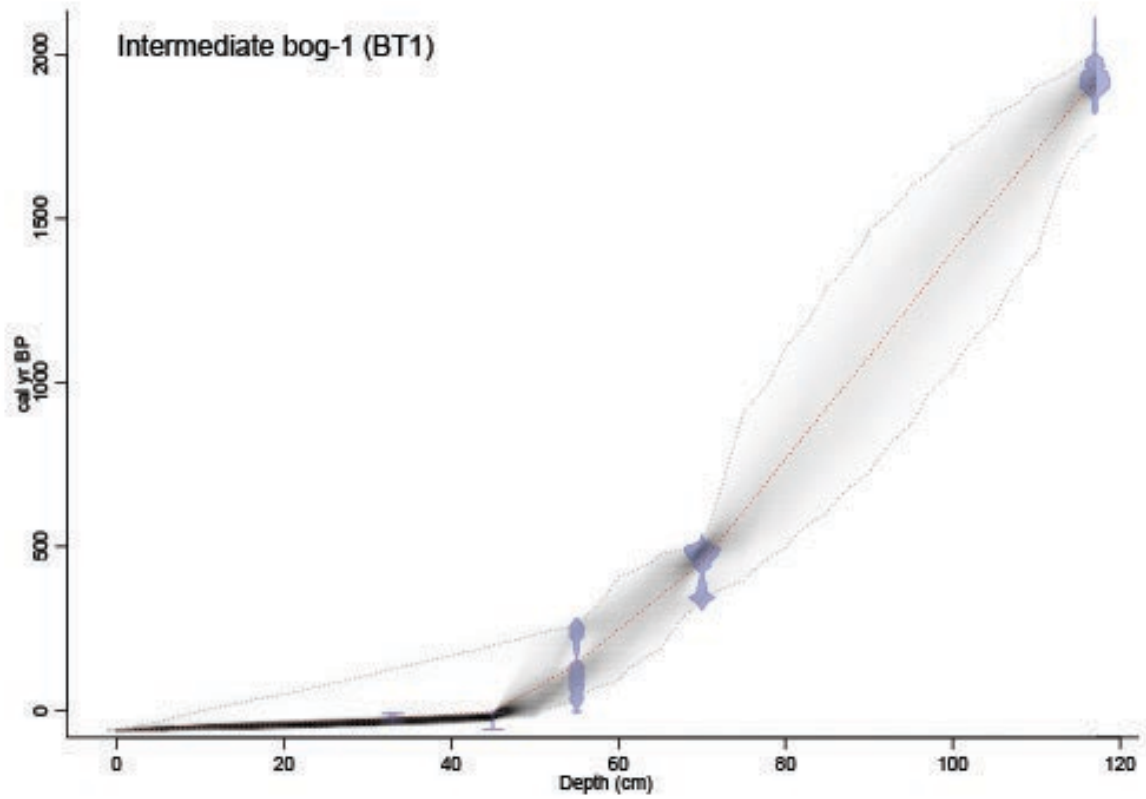
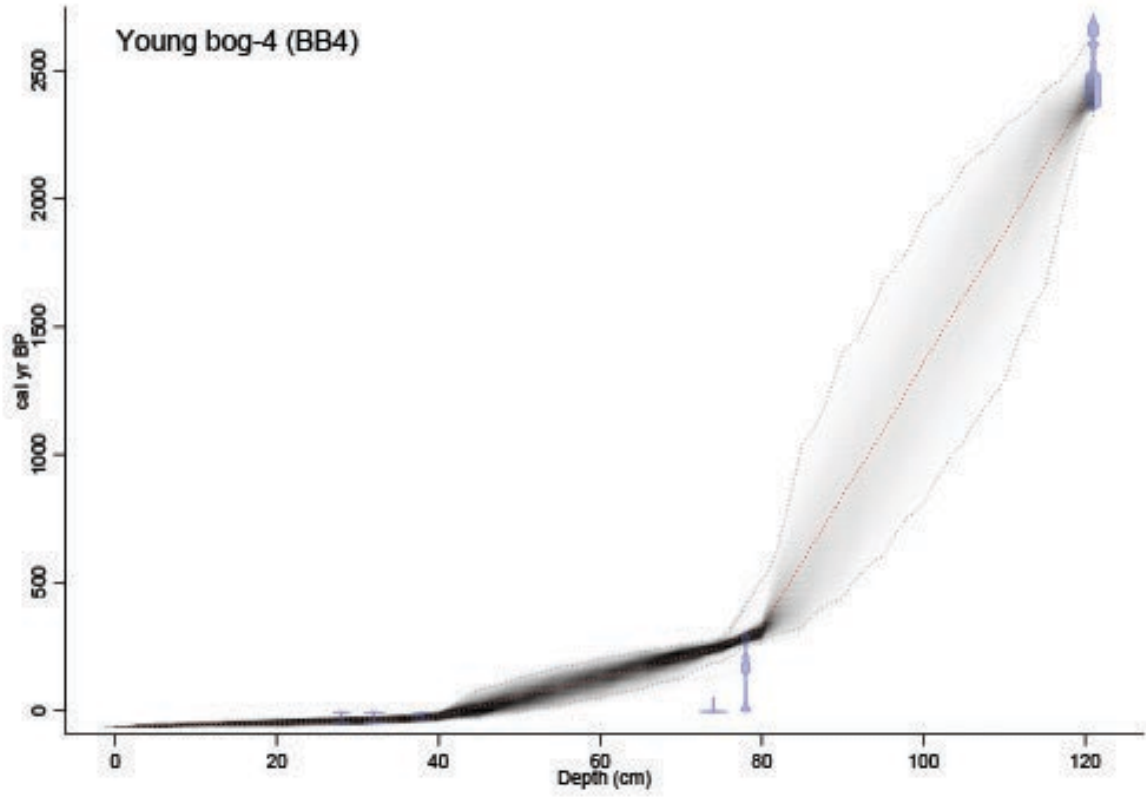


## SUPPLEMENTAL INFORMATION

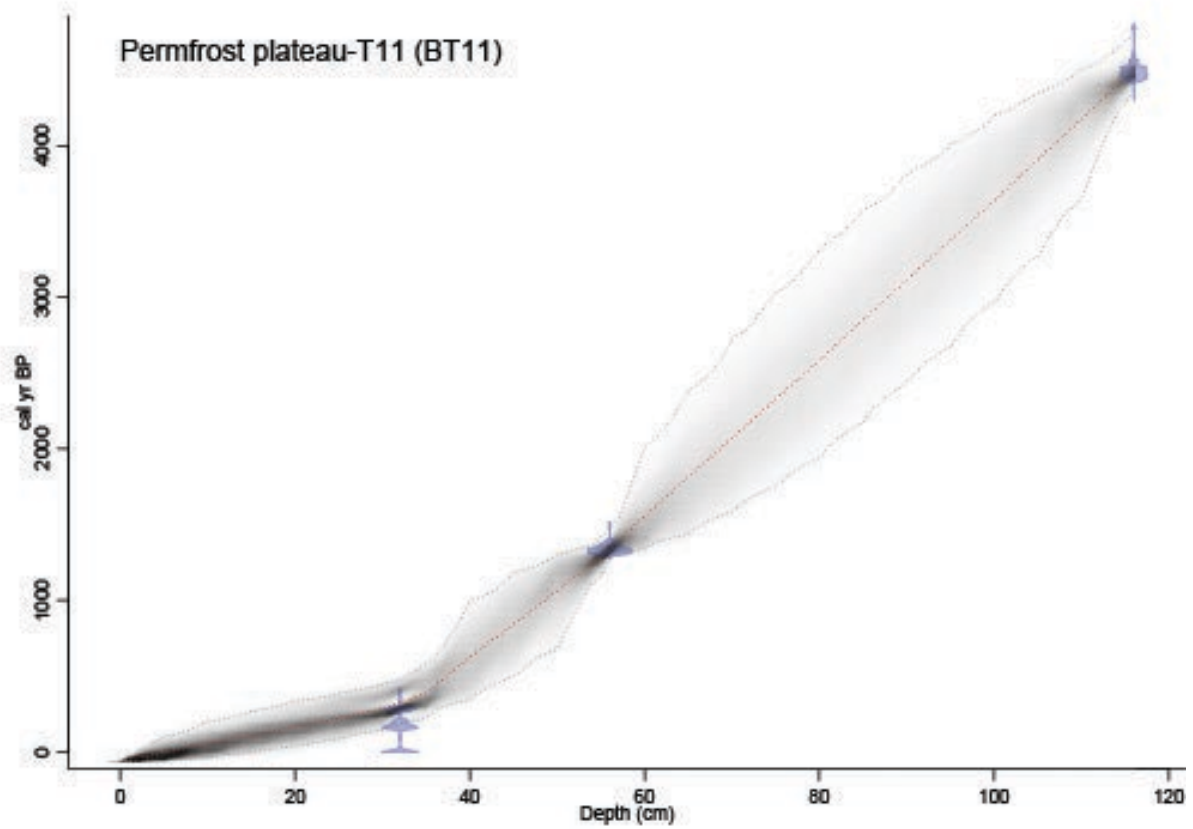
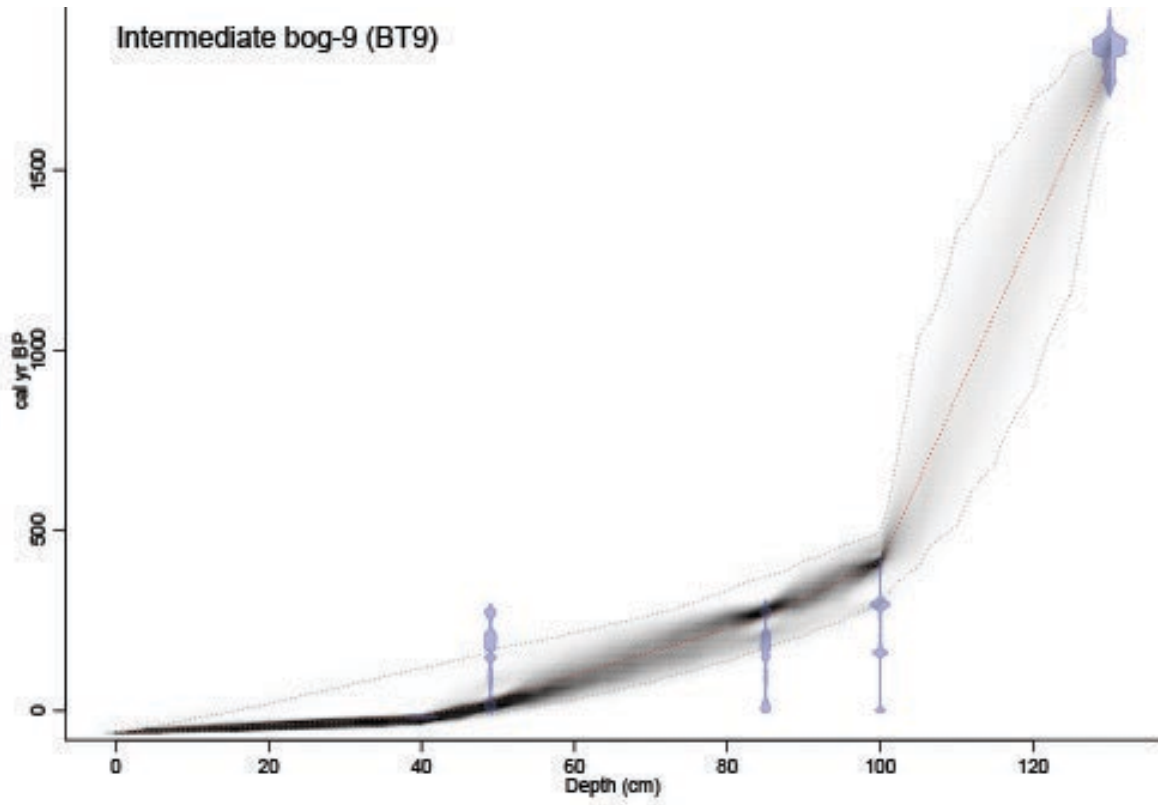
**Figure S8.** Results of Bacon age models (Blaauw & Christen, 2011) for each soil core using date of sampling for the surface and the  $^{14}\text{C}$  dates found in Table S2.



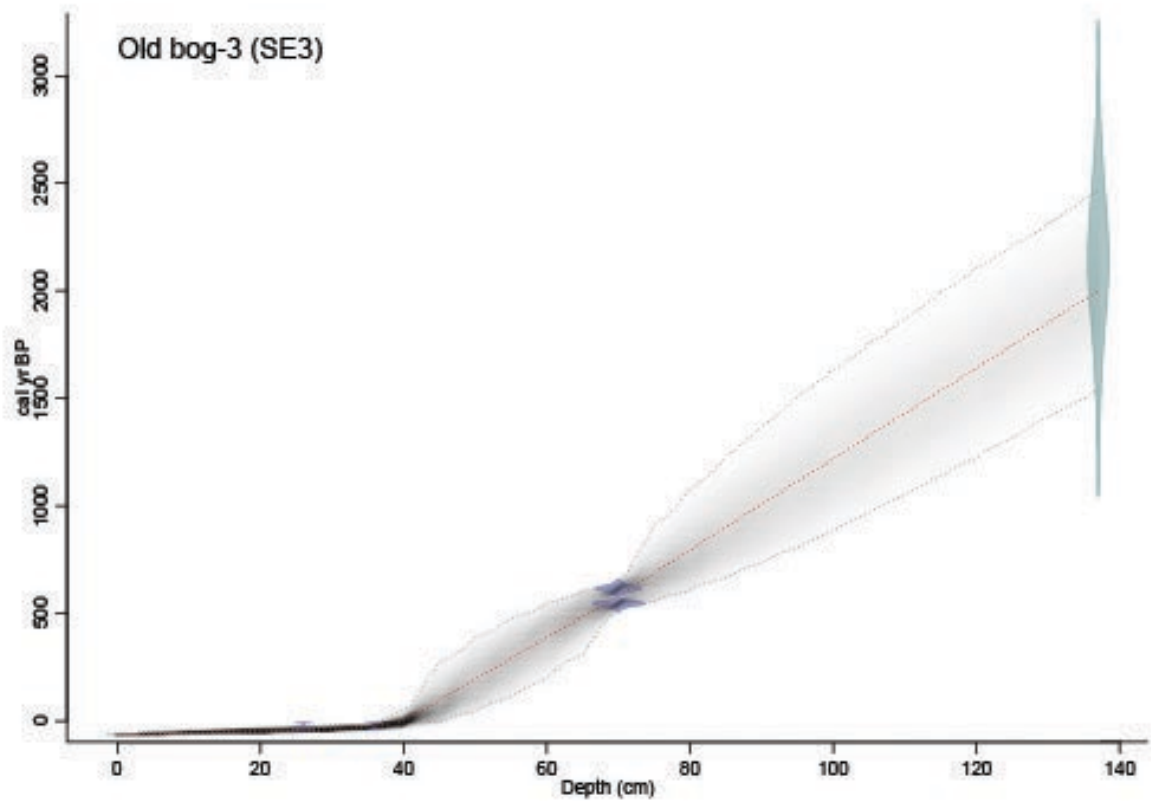
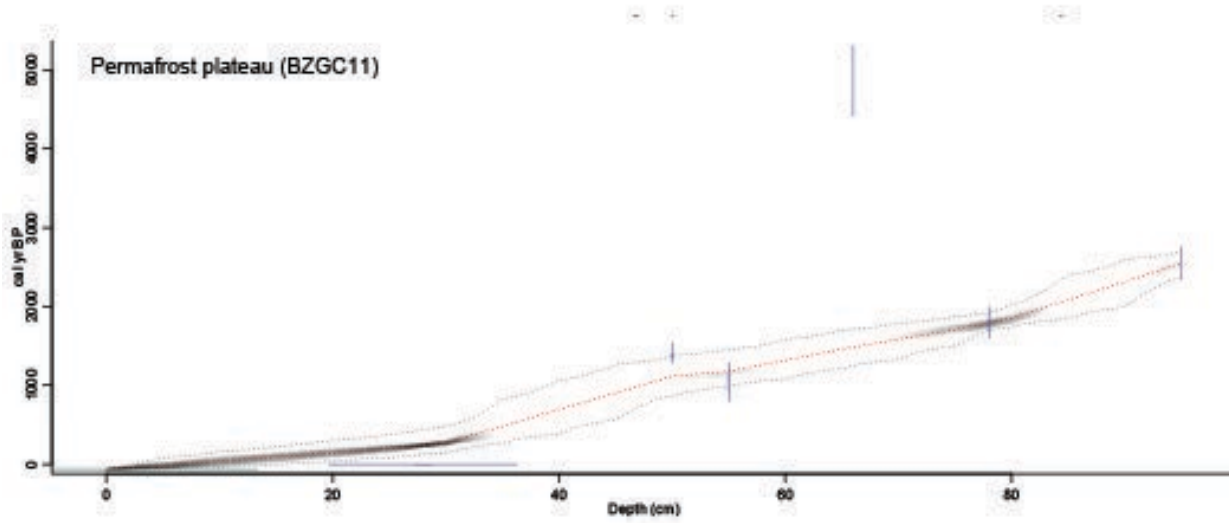
# SUPPLEMENTAL INFORMATION



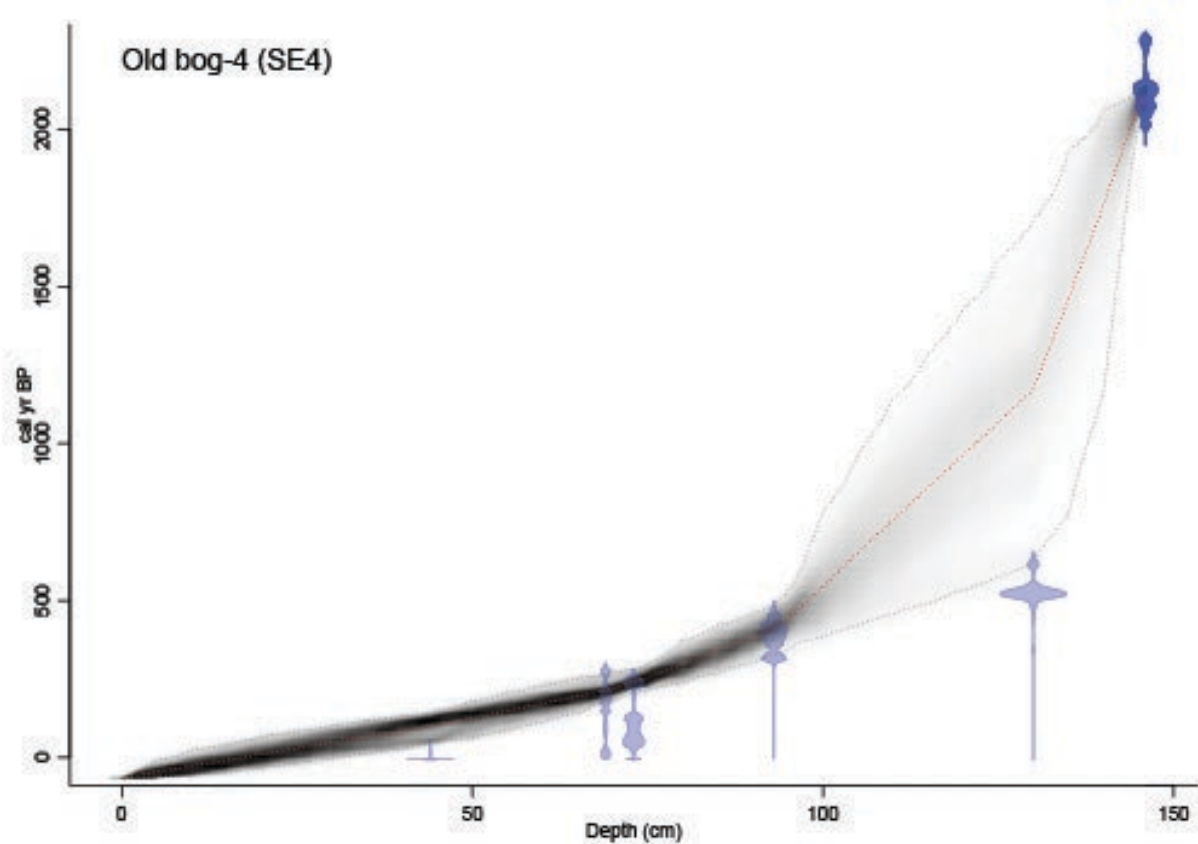
SUPPLEMENTAL INFORMATION



# SUPPLEMENTAL INFORMATION



## SUPPLEMENTAL INFORMATION



### References

- Blaauw, M., & Christen, J. Blaauw, M., & Christen, J. A. (2011). Flexible paleoclimate age-depth models using an autoregressive gamma process. *Bayesian Anal.*, 6(3), 457-474
- Hansson, S. V., et al. (2015). "Downwash of atmospherically deposited trace metals in peat and the influence of rainfall intensity: An experimental test." *Science of The Total Environment* 506–507: 95-101.
- Manies, K., Fuller, C., & Jones, M. (2016). *Modeling Peat Ages Using  $^7\text{Be}$  Data to Account for Downwash of  $^{210}\text{Pb}$* . Paper presented at the American Geophysical Union Fall Meeting, San Francisco, CA. <https://ui.adsabs.harvard.edu/abs/2016AGUFM.B23C0597M>.